OPEN ACCESS

Original research

Lysosomal lipid switch sensitises to nutrient deprivation and mTOR targeting in pancreatic cancer

Maria Chiara De Santis,[1] Luca Gozzelino ,[1] Jean Piero Margaria ,[1] Andrea Costamagna,[1] Edoardo Ratto,[1] Federico Gulluni,[1] Enza Di Gregorio,[1] Erica Mina,[1] Nicla Lorito,[2] Marina Bacci,[2] Rossano Lattanzio,[3] Gianluca Sala ,[3] Paola Cappello ,[1] Francesco Novelli,[1] Elisa Giovannetti,[4,5] Caterina Vicentini,[6] Silvia Andreani,[7] Pietro Delfino,[7] Vincenzo Corbo ,[6,7] Aldo Scarpa ,[6,7] Paolo Ettore Porporato,[1] Andrea Morandi,[2] Emilio Hirsch,[1] Miriam Martini [1]

► Additional supplemental material is published online only. To view, please visit the journal online (http://dx.doi.org/10.1136/gutjnl-2021-325117).

For numbered affiliations see end of article.

Correspondence to
Dr Miriam Martini, Dept. of Molecular Biotechnology and Health Sciences, University of Turin, Torino, Italy;
miriam.martini@unito.it

EH and MM contributed equally.

Received 10 May 2021
Accepted 7 May 2022
Published Online First
27 May 2022

To cite: De Santis MC, Gozzelino L, Margaria JP, *et al*. *Gut* 2023;**72**:360–371.

ABSTRACT

Objective Pancreatic ductal adenocarcinoma (PDAC) is an aggressive disease with limited therapeutic options. However, metabolic adaptation to the harsh PDAC environment can expose liabilities useful for therapy. Targeting the key metabolic regulator mechanistic target of rapamycin complex 1 (mTORC1) and its downstream pathway shows efficacy only in subsets of patients but gene modifiers maximising response remain to be identified.

Design Three independent cohorts of PDAC patients were studied to correlate PI3K-C2γ protein abundance with disease outcome. Mechanisms were then studied in mouse (KPC mice) and cellular models of PDAC, in presence or absence of PI3K-C2γ (WT or KO). PI3K-C2γ-dependent metabolic rewiring and its impact on mTORC1 regulation were assessed in conditions of limiting glutamine availability. Finally, effects of a combination therapy targeting mTORC1 and glutamine metabolism were studied in WT and KO PDAC cells and preclinical models.

Results PI3K-C2γ expression was reduced in about 30% of PDAC cases and was associated with an aggressive phenotype. Similarly, loss of PI3K-C2γ in KPC mice enhanced tumour development and progression. The increased aggressiveness of tumours lacking PI3K-C2γ correlated with hyperactivation of mTORC1 pathway and glutamine metabolism rewiring to support lipid synthesis. PI3K-C2γ-KO tumours failed to adapt to metabolic stress induced by glutamine depletion, resulting in cell death.

Conclusion Loss of PI3K-C2γ prevents mTOR inactivation and triggers tumour vulnerability to RAD001 (mTOR inhibitor) and BPTES/CB-839 (glutaminase inhibitors). Therefore, these results might open the way to personalised treatments in PDAC with PI3K-C2γ loss.

WHAT IS ALREADY KNOWN ABOUT THIS SUBJECT?

⇒ Pancreatic ductal adenocarcinoma (PDAC) is an aggressive and lethal disease characterised by poor response to current therapies.

WHAT ARE THE NEW FINDINGS?

⇒ In this work, we show that loss of PI3K-C2γ, a class II PI3K, promotes PDAC growth and prevents mechanistic target of rapamycin (mTOR) signalling deactivation, triggering cellular addiction to glutamine. Studying genetically engineered mice, we found that the proliferative advantage of tumours with PI3K-C2γ loss correlates with hyperactivation of the mTOR pathway and rewiring of glutamine metabolism. Mechanistically, PI3K-C2γ recruits Asap1 to the lysosome to repress mTORC1 activation in response to glutamine decrease. Importantly, loss of PI3K-C2γ in PDAC triggers cancer vulnerability to a combination of mTOR and glutaminase inhibitors.

HOW MIGHT IT IMPACT ON CLINICAL PRACTICE IN THE FORESEEABLE FUTURE?

⇒ Similar to glutamine starvation, loss of PI3K-C2γ increases sensitivity to glutaminase inhibitors, CB-839 and BPTES, especially when in combination with everolimus. Our findings unravel a signal transduction pathway that contributes to glutamine dependence, representing an exploitable vulnerability for the development of effective therapeutic strategies for PDAC.

INTRODUCTION

Pancreatic ductal adenocarcinoma (PDAC) is on path to become the second leading cause of cancer-related death by 2030.[1] Resistance to chemotherapies represents a critical challenge for patients with pancreatic cancer, thus, novel therapeutic approaches for PDAC are urgently needed. A phenomenon contributing to therapeutic resistance and dismal prognosis is a unique characteristic of PDAC called desmoplasia, which results in reduced availability of oxygen and nutrients to the cancer. To survive in such a harsh microenvironment, pancreatic cancer cells adopt unique metabolic processes to meet their energy demand, including rewired glucose and glutamine metabolism.[2 3] Previous evidence demonstrates that glutamine is a

critical nutrient for pancreatic cancer,[4 5] being the major source of carbon and nitrogen for biosynthetic reactions and redox homeostasis.[6 7]

A key regulator of metabolic adaptation to nutrient availability is the mTOR (mechanistic target of rapamycin) pathway, which drives metabolic reprogramming to support biosynthetic needs and optimal cell growth. mTOR signalling is often dysregulated in PDAC, thus representing an attractive therapeutic target with remarkable responses in preclinical models.[8] However, results of clinical trials using mTOR inhibitors are less encouraging, showing clinical benefit only in a minority of PDAC patients.[9 10] Therefore, stratification of patients with genetic markers modifying susceptibility to mTOR inhibition is expected to provide a better therapeutic response.[11]

While it is well known that the mTOR axis is activated by class I PI3K,[12] class II PI3K play an opposite effect and their lipid product PI(3,4)P2 can act as a negative regulator of mTOR signalling.[13–15] Class II PI3Ks consist of three isoforms, PI3K-C2α, PI3K-C2β and PI3K-C2γ, which display non-redundant cellular roles and distinct biological functions.[16] The PI3K-C2γ isoform has a unique pattern of expression, appearing in liver, kidney and exocrine pancreas.[17] While the presence of PI3K-C2γ in the pancreas might suggest a role in PDAC, whether this lipid kinase affects cancer initiation and/or progression is still unclear.

In this study, we showed that loss of PI3K-C2γ accelerates PDAC development and progression with hyperactivation of the mTOR pathway. Our results showed that PI3K-C2γ inhibits mTORC1 through a specific mechanism, distinct from that of PI3K-C2β[13 14] and involving the PI(3,4)P2/Asap1/Arf1 pathway. This negative feedback is triggered by low glutamine and its loss in PDAC drives to glutamine addiction. Accordingly, lack of PI3K-C2γ sensitises PDAC cells to a synergic effect of combined mTOR and glutaminase (GLS1) inhibition in vitro and in vivo. Our findings thus support the notion that loss of PI3K-C2γ in PDAC might allow a more accurate patient stratification required to improve the therapeutic responses.

MATERIAL AND METHODS

Histopathological analysis

PI3K-C2γ protein expression was evaluated in three independent cohorts of PDAC samples. Sections were stained with specific antibodies: PIK3C2G (ThermoFisher, PA5-15239), phospho-S6 Ser235/236 (#4858, Cell Signalling), PCNA 6D645 (sc-71858) and phospho-4E-BP1 Thr37/46 (#2855, Cell Signalling). For mouse analysis, PanIN was defined by previously published guidelines in genetically modified mouse models of PDAC.[18 19]

Mice strains generation and analysis

B6/C57 *Pik3c2g*$^{-/-}$ mice were previously generated.[17] Kras$^{LSL\text{-}G12D}$;Trp53$^{LSL\text{-}R172H}$ (KP)[18] and Pdx-Cre mice were kindly provided by prof. Franco Novelli and prof. Paola Cappello. *Pik3c2g*$^{+/+}$ (WT) and *Pik3c2g*$^{-/-}$ (KO) mice were crossed with KP and Pdx-Cre mice to generate all experimental cohorts. Nu/nu CD1^{+} mice were purchased from Charles River Laboratories. All animal experiments were authorised by the Italian Ministry of Health (33/2019-PR). MRI scans were acquired at 7.1T on a Bruker Avance Neo 300 spectrometer equipped with the Micro 2.5 microimaging probe. For orthotopic injections, KPC cells (10^6 cells) were injected into 8 weeks old *Pik3c2g*$^{+/+}$ mice. For BPTES (12.5 mg/kg/mice, twice a week) and/or everolimus (1.5 mg/kg/mice, daily) treatment, KPC (2×10^6 cells/mice) and Panc1 (4×10^6 cells/mice) cells were injected subcutaneously in nu/nu CD1^{+} mice.

Cell culture

The human PC cell lines Capan1 (HBT-79), MiaPaca2 (CRL-1420), Panc1 (CRL-1469) and Cos7 (CRL-1651) cell lines were purchased from American Tissue Cell Culture (Manassas, Virginia, USA) and maintained under culture with DMEM (Gibco) High Glucose containing 2 mM glutamine (Invitrogen), 5000 U/mL Penicillin-Streptomycin (Gibco) and 10% heat-inactivated dialyzed fetal bovine serum (Invitrogen). For drug treatment, Everolimus (11597, Cayman Chemical), CB-839 (22038, Cayman Chemical) or BPTES (S7753, Aurogene) were added the day after seeding in culture media. Cells were counted at the indicated time point with CellTiter-Fluor Cell Viability Assay (Promega). Human cell lines authentication was performed by BMR Genomics. All cell lines were routinely tested for Mycoplasma contamination using PCR.

Metabolic assay

The media were assayed for glucose and lactate levels by using Biosen C-Line analyser according to the manufacturer's instruction. KPC WT and KO cells were subjected to the Seahorse XF Cell Mito Stress Test. To analyse the incorporation of uniformly (U) radiolabeled ^{14}C-glutamine into proteins and lipids, culture medium was supplemented with 0.05 µCi/mL ^{14}C-glutamine (Perkin Elmer).

Statistical analysis

Prism software (GraphPad) was used for statistical analysis. CompuSyn software was used to score the Combination Index of the combinatorial treatment. Significance was calculated with Student's t-test and one-way or two-way analysis of variance tests followed by Bonferroni's post hoc analysis or Mantel Cox log-rank test where appropriate.

RESULTS

PI3K-C2γ expression is reduced in pancreatic PDAC

To assess the relevance of PI3K-C2γ expression in cancer, we interrogated PDAC transcriptomes available at cBioPortal for Cancer Genomics.[20 21] Data from TCGA cohort (n=148) showed that shallow deletion (heterozygous loss), but rarely mutations, of *PIK3C2G* is a common aberration in about 15% of PDAC patients.[20 21] In addition, gene expression analysis performed in four integrated PDAC datasets showed that *PIK3C2G* is mainly expressed in neoplastic epithelial cells (online supplemental figure S1A), indicating that the reduced expression of *PIK3C2G* observed in the TCGA and ICGC datasets is due to a decreased expression in tumour but not stromal cells.[22–25] Furthermore, we observed a significant negative correlation (Spearman: −0.51; p=2.22e-13) between *PIK3C2G* methylation and mRNA expression, consistent with a reduction of its expression in PDAC patients.[20 21]

Next, we explored the expression of *PIK3C2G* in the context of the two molecular subtypes of PDAC, using the Moffitt's PDAC classification.[26] We found that *PIK3C2G* expression is significantly lower in the aggressive basal-like subtype than in the classical PDAC,[27 28] in both the TCGA (n=148, p=0.035) and the ICGC cohorts (n=95, p=0.013) (online supplemental figure S1B). We also investigated the correlation between the expression of *PIK3C2G* and the surrogate biomarker of classical PDAC cells, GATA6, confirming the enrichment of PI3K-C2γ low expressors in GATA6 low tumours in both cohorts (online supplemental figure S1C).

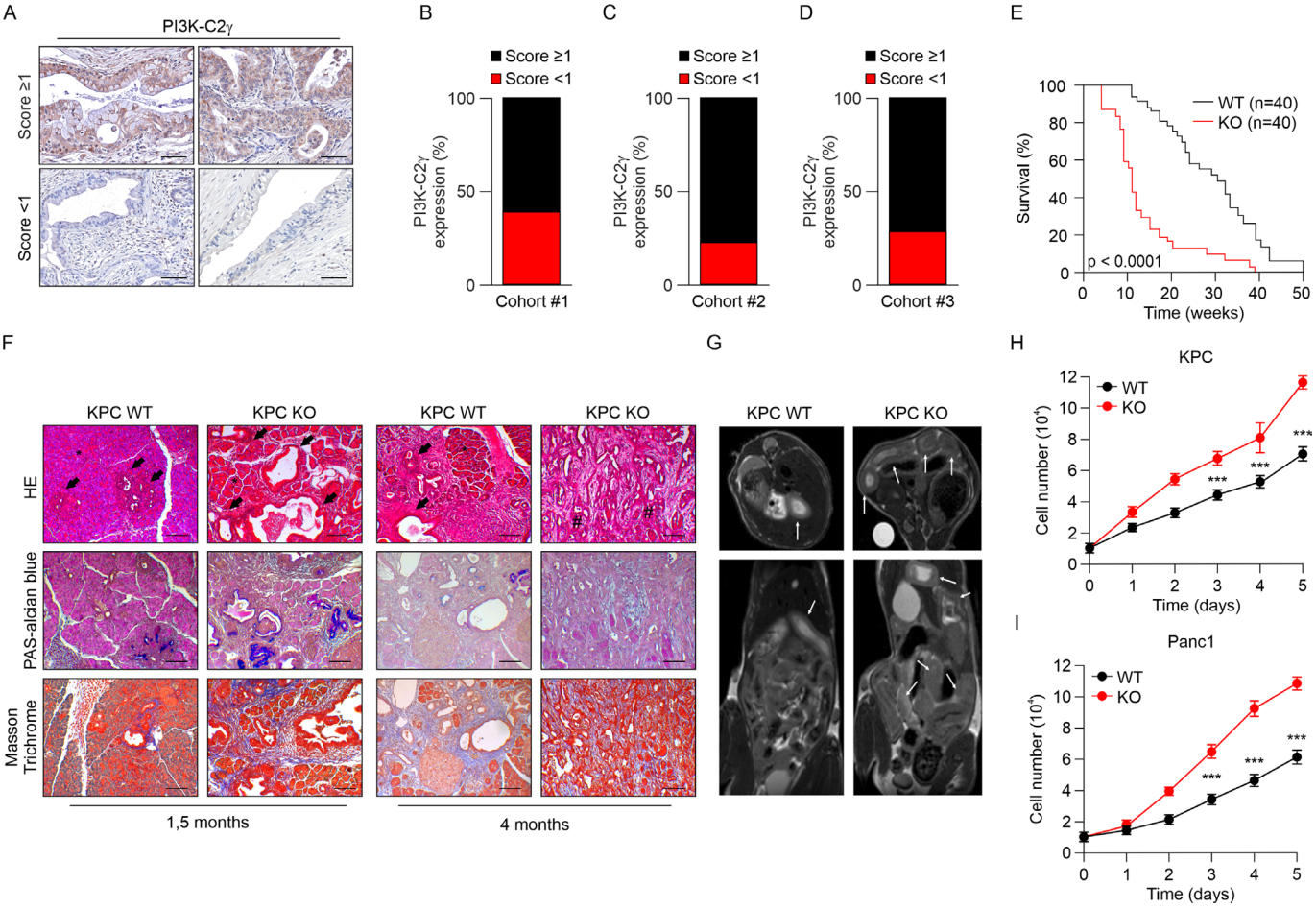

Figure 1 PI3K-C2γ loss decreases KPC mice survival and accelerates PDAC cells growth. (A, B) Immunohistochemical (IHC) assessment (A) and quantification (B) of the level of PI3K-C2γ expression in PDAC patients in cohort #1. Representative images of high (score ≥1) and low (score <1) PI3K-C2γ expressing tumours (n=73) (scale bar=100 µm). (C, D) Percentage of tumours expressing high (score ≥1) or low (score <1) levels of PI3K-C2γ in cohort #2 (n=76), (C) and cohort #3 (n=45), (D). (E) Kaplan-Meier curve for survival of WT/KO KPC mice (n=40, Mantel-Cox log-rank test). (F) Histopathological analysis of WT/KO KPC mice pancreata. Representative H&E images, PAS-alcian blue and Masson trichrome stainings of 1.5 and 4 months old mice. Arrows indicate PanIN lesions, asterisks (*) indicate normal acini, hashtags (#) indicates PDAC (scale bar=100 µm). (G) Axial (top) and coronal (bottom) T_{2w} MRI (B_0=7.1 T) of WT (left) and KO (right) 6 weeks old KPC mice. White arrows indicate pancreatic tumour. (H, I) Growth assay of WT/KO KPC (H) and Panc1 (I) cells (n=5). Data are shown as mean±SEM, ANOVA followed by Bonferroni's post hoc test, otherwise indicated. ANOVA, analysis of variance; KPC, LSL-KrasG12D/+;LSL-Trp53R172H/+;Pdx-1-Cre; PAS, Periodic acid–Schiff; PDAC, pancreatic ductal adenocarcinoma.

To confirm that a subset of PDAC shows reduced PI3K-C2γ expression, we used a validated antibody to stain by IHC a total of 194 cases from three independent cohorts. The specificity of the antibody for PI3K-C2γ was validated in pancreas tissue from PI3K-C2γ-deficient *Pik3c2g*$^{-/-}$ mice[17] (online supplemental figure S1D). In the first cohort (cohort #1, n=73), low levels of PI3K-C2γ were found in 38% (28/73) of patients (IHC score <1), while 62% were classified as positive (IHC score ≥1) (figure 1A and B). Moreover, the reduction of PI3K-C2γ expression was observed in 35.6% (16/45) of moderately differentiated PDACs and 42.9% (12/28) of poorly differentiated PDACs (online supplemental figure S1E). In a second independent cohort (cohort #2, n=76), low levels of PI3K-C2γ were found in 22.4% (17/76) of patients, 46.9% (23/49) of which were scored as poorly differentiated PDAC (figure 1C). In the third cohort (cohort #3, n=45), low levels of the protein were detected in 33.3% (15/45) of PDAC patients (figure 1D), 40.0% (4/10) of which scored as poorly differentiated PDAC (online supplemental table S1). Patients with a low expression of PI3K-C2γ exhibited significantly shorter clinical overall survival (but not progression-free survival) than those with high PI3K-C2γ levels (p=0.035, online supplemental figure S1F,G).

Loss of PI3K-C2γ promotes pancreatic cancer in mice

To investigate the role of PI3K-C2γ in pancreatic cancer development, we crossed *Pik3c2g*$^{-/-}$ mice[17] with LSL-KrasG12D/+;LSL-Trp53R172H/+;Pdx-1-Cre (KPC WT)[18] and generated KPC KO mice. While KPC WT mice succumbed to death at an average of 30 weeks, animals from KPC KO group died at an average of 11 weeks of age (p<0.0001, figure 1E), thus indicating that the loss of PI3K-C2γ reduces overall survival time. However, mice lacking the expression of PI3K-C2γ in WT background[17] were not prone to tumour development and did not display metabolic alterations (ie, pancreatic, liver and renal functions) (online supplemental figure S1H and online supplemental table S2).

Analysis of PanIN lesions indicated that loss of PI3K-C2γ promotes the appearance of each stage of PanIN progression (PanIN1, 2, and 3) (figure 1F and online supplemental figure S1I,J). This disease acceleration was not associated with metabolic alterations, as no

changes in blood glucose were detected in both genotypes up to 8 weeks (online supplemental figure S1K). In further agreement with accelerated lethality in the absence of PI3K-C2γ, T_{2w} MRI analysis, indicated that KPC KO tumours were more diffuse throughout the abdomen than KPC WT controls (figure 1G). In line with this finding, KPC KO mice showed a significant increase in the number of lung and liver metastases (online supplemental figure S2A).

In addition, reimplantation of primary tumour cells derived from WT and KO tumours (online supplemental figure S2B) in syngeneic mice indicated that KPC KO tumours grew at a significantly increased rate and developed more metastases than WT controls (online supplemental figure S2C,D). Accordingly, KPC KO cells showed increased cell growth and invasive ability than WT cells, thus supporting that the absence of PI3K-C2γ provides a cell-autonomous growth advantage (figure 1H and online supplemental figure S2E).

To assess the functional impact of PI3K-C2γ in human PDAC cells, we knocked out the PIK3C2G gene using CRISPR/Cas9 in three PDAC cell lines (Panc1, Capan1 and MiaPaca2). As for mice, the endogenous PI3K-C2γ could not be detected by Western blot but the nature of the knock-out was confirmed by RT-PCR (online supplemental figure S2F-H) as well as immunohistochemistry (online supplemental figure S2I). PI3K-C2γ-deficient Panc1, Capan1 and MiaPaca2 cells showed significantly higher cell numbers than WT controls (figure 1I and online supplemental figure S2J,K). In addition, we observed increased ERK signalling (online supplemental figure S2L,M) in PI3K-C2γ-deleted cells in line with their enhanced cell number. Finally, increased proliferation in human and murine KO cells was confirmed in PCNA-stained sections from either KPC tumours (figure 2A) or xenograft models (online supplemental figure S3A).

These findings in PI3K-C2γ-deficient PDAC cells suggested an intrinsic defect in signalling pathways controlling cell growth and, in support to this hypothesis, phosphorylation of mTORC1 pathway effectors, like S6K and 4EPB1, was found higher in murine KPC KO than in WT controls (online supplemental figure S3B). In further agreement, human KO cells also displayed abnormally elevated mTORC1 pathway activation, as per increased 4EBP1 and S6K phosphorylation (online supplemental figure S3C,D).

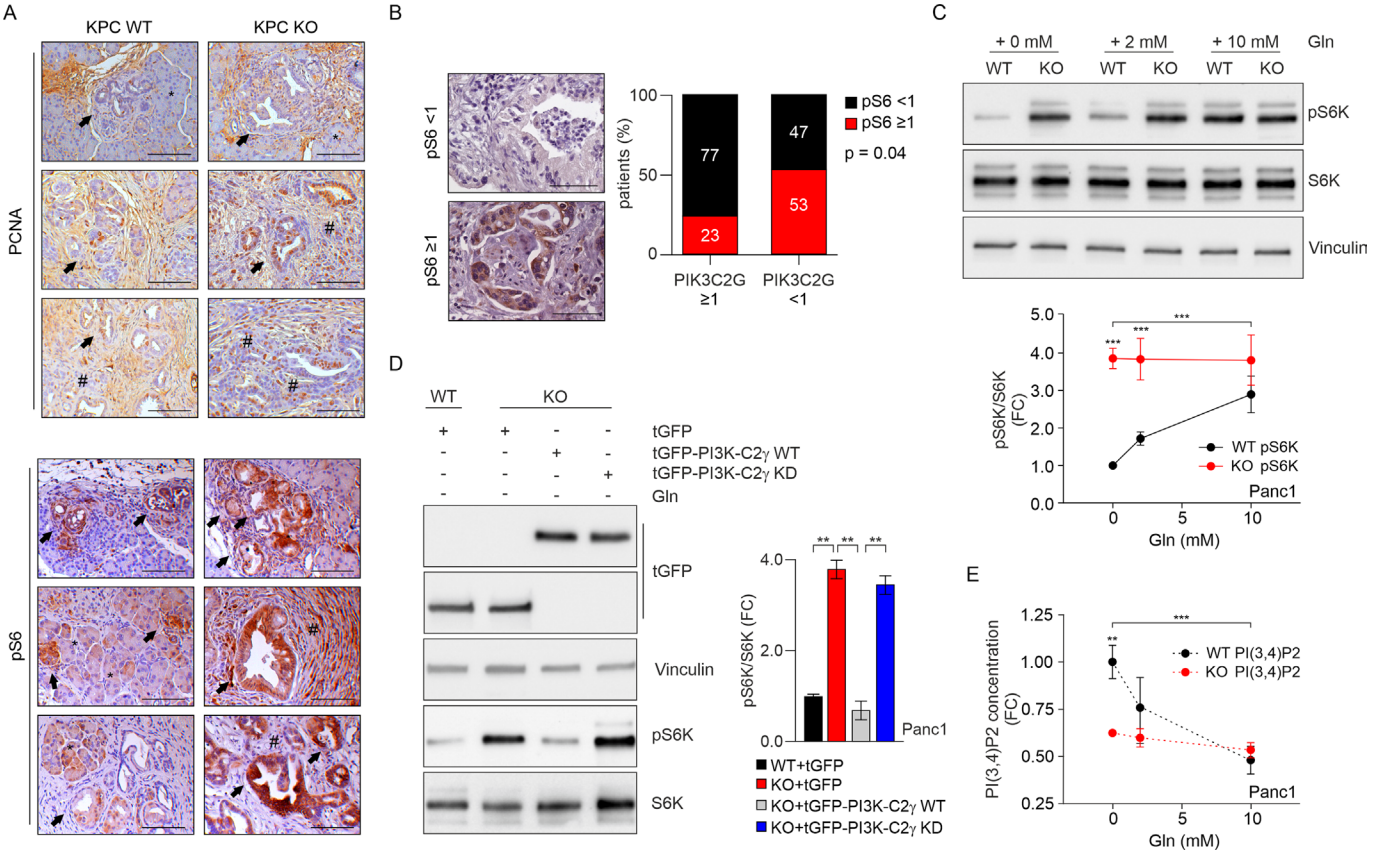

Figure 2 PI3K-C2γ loss induces mTORC1 hyperactivation on glutamine deprivation. (A) IHC assessment of the level of PCNA (top) and pS6 (bottom) in tumours taken from WT/KO KPC mice. Arrows indicate PanIN lesions, asterisks (*) indicate normal acini, hashtags (#) indicates PDAC (scale bar=100 µm). (B) IHC assessment (left) and quantification (right) of the level of pS6 expression (focal positive reactivity) in PDAC patients (scale bar=100 µm) expressing high (score ≥1) or low (score <1) of PI3K-C2γ levels (n=45 patients, p=0.04, χ^2 test). (C) WB analysis of mTORC1 activity in WT/KO Panc1 cells that were starved of glutamine (Gln), then stimulated with Gln at the indicated concentrations. Representative Western blot images of whole-cell lysates probed with indicated antibodies (top) and quantification of pS6K/S6K ratio in the indicated conditions (n=9, bottom). (D) WB analysis of pS6K in WT Panc1, KO Panc1 or KO Panc1 cells re-expressing WT or the kinase dead (KD) versions of tGFP-PI3K-C2γ after glutamine depletion for 2 hours. Representative Western blot images of whole-cell lysates probed with indicated antibodies (left) and quantification of pS6K/S6K ratio in the indicated conditions (n=4, right). (E) Quantification of PI(3,4)P2 concentration in WT/KO Panc1 cells that were starved of glutamine (Gln), then stimulated with Gln at the indicated concentrations (n=5). Data are shown as mean±SEM, ANOVA followed by Bonferroni's post hoc test, otherwise indicated. ANOVA, analysis of variance; IHC, immunohistochemical; mTORC1, mechanistic target of rapamycin complex 1; KPC, LSL-KrasG12D/+;LSL-Trp53R172H/+;Pdx-1-Cre; PCNA, proliferating cell nuclear antigen; PDAC, pancreatic ductal adenocarcinoma. **P<0.01; ***p<0.001.

PI3K-C2γ kinase activity is critical for mTORC1 repression upon glutamine deprivation

We next assessed phosphorylation of mTORC1 downstream effectors like 4EBP1 and S6 by immunohistochemistry in PDAC samples. In tumours with PI3K-C2γ score <1, 4/12 PDAC cases (33.3%) were phospho-4EBP1 positive while in tumours with PI3K-C2γ score ≥1, 6/25 PDAC cases (24.0%) were phospho-4E-BP1 positive (online supplemental figure S3E). We observed a trend towards increased p4E-BP1 and reduced PI3K-C2γ expression or increased pS6 but the correlation was not significant. A stronger proof of mTORC1 pathway activation was evidenced in the staining for pS6, where a significant negative association between pS6 and PI3K-C2γ (n=45, p=0.04 by χ^2 test) was found in PDAC patients stratified for PI3K-C2γ expression (figure 2B and online supplemental figure S3F). Similarly, pS6 appeared more pronounced in sections of KPC KO murine tumours than in WT controls (figure 2A), thus indicating that, on loss of PI3K-C2γ, mTORC1 hyperactivation occurs in both human and murine PDAC samples.

Therefore, we tested how the loss of PI3K-C2γ impacted on mTORC1 signalling in PDAC by analysing upstream modulators and downstream effectors in different growth conditions. First, we tested whether activation by serum of the PI3K-dependent mTORC1 activators Akt1 and Akt2 was different in WT and KO cells as well as in KO cells reconstituted with WT or kinase dead (KD) PI3K-C2γ. Either the loss of PI3K-C2γ or its re-expression did not affect Akt1/2 phosphorylation in all conditions tested (online supplemental figure S4A-D), thus suggesting a more direct action, potentially compatible with the PI3K-C2γ product PI(3,4)P2 directly inhibiting mTORC1.[13 14] Next, phosphorylation of S6K in response to serum deprivation was analysed and found potently reduced in both genotypes (online supplemental figure S3C,D). However, pS6K remained slightly higher in rapidly growing KO cells independently of the presence or absence of serum (online supplemental figure S3C,D). Activity of the mTORC1 complex can also be regulated by amino acids[29] and, in WT cells, decreasing glutamine concentration caused a dose-dependent reduction of serum-induced S6K phosphorylation (figure 2C, online supplemental figures S3B-D and S4E (input)). On the contrary, when KO cells were grown in the presence of serum but in limiting amounts of glutamine, pS6K remained high regardless of glutamine levels (figure 2C, online supplemental figures S3B-D and S4E (input)), thus suggesting that loss of PI3K-C2γ removes an inhibiting action on mTORC1 signalling in response to glutamine deprivation. In agreement with this hypothesis, the catalytic activity of the mTORC1 complex, assessed in a kinase assay in the absence of glutamine, was higher in KO cells than in WT controls (online supplemental figures S4E,F). In the same conditions of glutamine deprivation, add-back of the WT but not of the KD form of PI3K-C2γ restored pS6K levels (figure 2D). Moreover, when glutamine was withdrawn from WT cells maximal production of PI(3,4)P2 (figure 2E), a PI3K-C2γ product[17] able to inhibit mTORC1 activity,[13] occurred together with the strongest reduction of S6K phosphorylation (figure 2C). Conversely, loss of PI3K-C2γ significantly blunted the synthesis of this phosphoinositide in response to low glutamine and kept pS6K constitutively high, thus demonstrating that PI3K-C2γ is required to produce the mTORC1 negative regulator PI(3,4)P2 in the absence of glutamine in murine and human PDAC cells (figure 2C and E and online supplemental figure S4G). Altogether, these observations support a model where glutamine deprivation leads to the accumulation of a PI3K-C2γ-generated pool of PI(3,4)P2 that in turn reduces mTORC1 activity, likely to fine tune protein synthesis with amino acid availability.

PI3K-C2γ lipid product recruits ASAP1 on lysosomes upon glutamine depletion

In line with the increased phosphorylation of S6K on glutamine withdrawal, PI3K-C2γ loss enhanced mTOR localisation on lysosomes (online supplemental figure S4H-I), where mTORC1 activation preferentially occurs.[30] Next, PI3K-C2γ subcellular localisation was tested in WT Panc1 or Cos7 cells cotransfected with tGFP-PI3K-C2γ and miRFP-Lamp1. The number of PI3K-C2γ-Lamp1 positive structures significantly increased on glutamine withdrawal (figure 3A and B and online supplemental figure S5A,B), thus indicating that PI3K-C2γ is enriched at the lysosome on glutamine deprivation. Next, to verify that PI3K-C2γ lipid kinase activity occurs on lysosomes, tGFP-PI3K-C2γ−miRFP-Lamp1 cells were cotransfected with the fluorescent sensor NES-mCherry-cPHX3 specifically detecting PI(3,4)P2. Colocalisation of the three signals was observed in live cell imaging, indicating that, in the absence of glutamine, PI3K-C2γ exerts its catalytic activity on the lysosome to restrain mTORC1 activation (figure 3C,D and online supplemental figure S5C-F).

Given that glutamine-mediated mTORC1 activation depends on the nucleotide cycling of the small GTPase ADP ribosylation factor-1 (Arf1),[31 32] we tested whether PI3K-C2γ is required for the transition of Arf1 to the inactive state. Pull-down experiments of the GTP-bound active form of Arf1 demonstrated that the loss of PI3K-C2γ is associated with elevated Arf1 activity in cell models (figure 3E–H and online supplemental figure S5G) and in tumours derived from xenograft experiments (online supplemental figure S5H,I). To further verify that the lipid product generated by PI3K-C2γ is required to regulate Arf1 activity, we re-expressed a KD PI3K-C2γ in KO models. While the exogenous re-expression of WT PI3K-C2γ is sufficient to deactivate Arf1 (figure 3G and H) and to limit mTOR (figure 2D), expression of the KD mutant fails to change Arf1 activity (figure 3G and H).

We next hypothesised that PI(3,4)P2 could constitute a docking site for Asap1 (ArfGAP with SH3 domain, ANK repeat and PH domain-containing protein), a GAP protein required for Arf1 inhibition.[33 34] Using confocal imaging, we found that Asap1 and PI3K-C2γ colocalised on Lamp1 positive vesicles on glutamine depletion (figure 4A,B). On the contrary, Asap1 failed to localise at the lysosomes when cotransfected with PI3K-C2γ KD mutant in response to glutamine starvation (figure 4C,D). Consistently, loss of PI3K-C2γ reduced the colocalisation of Asap1 with Lamp1 (online supplemental figure S6A). In addition, we found that Asap1 colocalises with PI(3,4)P2 (detected by the NES-mCherry-cPHX3 probe) on Lamp1 positive vesicles in live imaging experiments (figure 4E,F).

To demonstrate that PI3K-C2γ-derived PI(3,4)P2 is responsible for the regulation of the Asap1-Arf1 axis, we showed that Asap1 can associate not only with PI(4,5)P2, as previously reported,[34] but also with PI(3,4)P2 (online supplemental figure S6B,C). As expected, the absence of Asap1 elevated the levels of the active Arf1 (figure 4G) but re-expression of PI3K-C2γ did not rescue active Arf1 levels, indicating that PI3K-C2γ is epistatic to Asap1 (figure 4G). In line with Arf1 activation, pS6K levels were higher in Asap1 KO cells compared with WT controls (figure 4G). To further verify that the interaction between the lipid product PI(3,4)P2 and Asap1 is required for regulating Arf1 activity, we mutagenised the PH domain of Asap1 (R345L) to disrupt the ability to interact with PI(3,4)P2,[35] but not PI(4,5)P2 (online

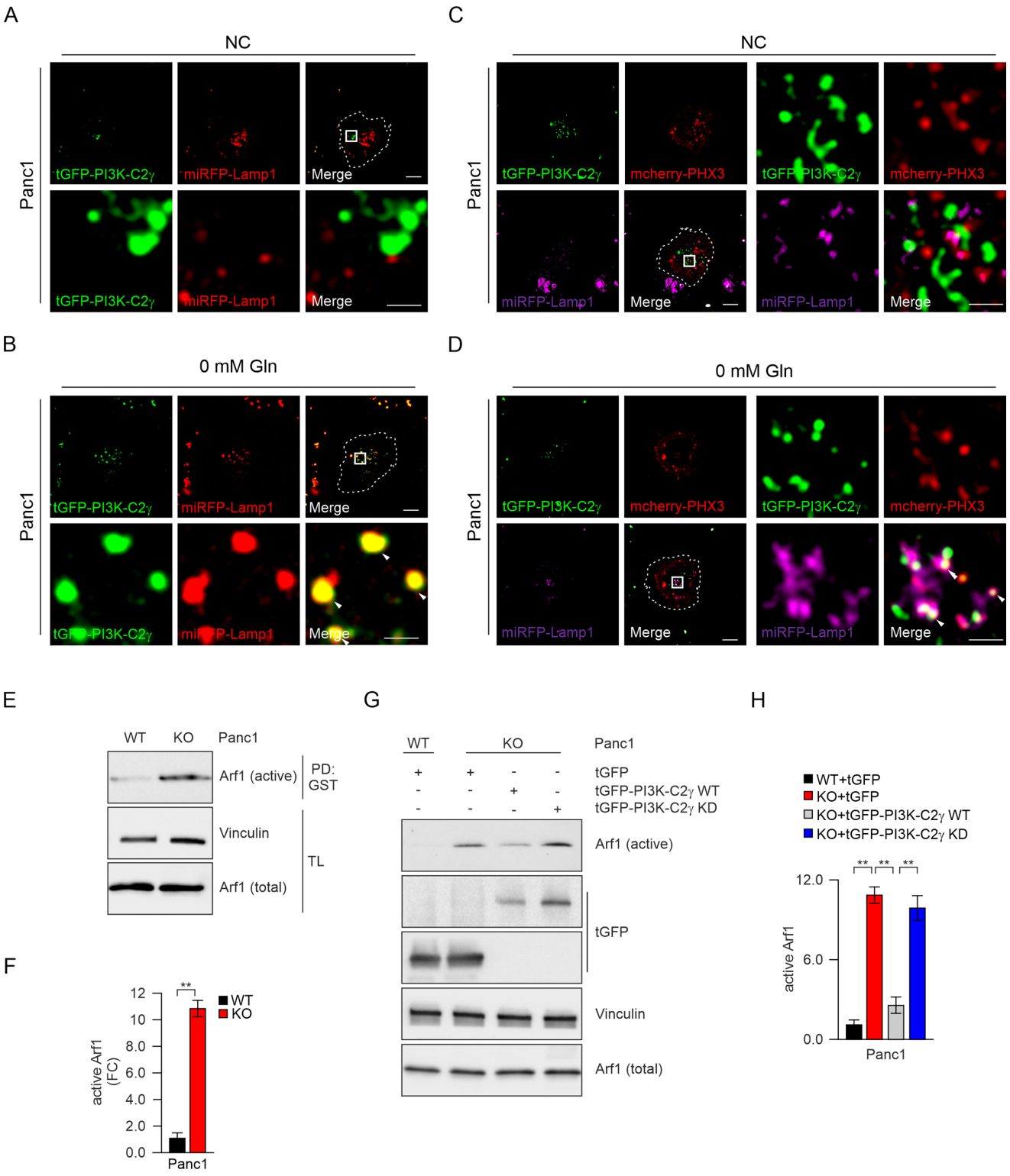

Figure 3 PI3K-C2γ-derived PI(3,4)P2 inhibits Arf1 activity. (A, B) Localisation of PI3K-C2γ on Lamp1-positive lysosomes. Representative confocal images of tGFP-labelled PI3K-C2γ and miRFP-labelled LAMP1 in normal culture conditions (NC), (A) or on glutamine withdrawal (0 mM Gln), (B) for 2 hours in Panc1 cells. Dashed white line defines cell limits. White arrows indicate colocalisation of the indicated proteins (scale bar=10 µm). (C, D) Localisation of PI3K-C2γ and PI(3,4)P2 on Lamp1-positive lysosomes. Representative confocal images of tGFP-labelled PI3K-C2γ, mCherry-labelled PHX3 (probe for the detection of PI(3,4)P2) and miRFP-labelled LAMP1 in normal culture conditions (NC), (C) or on glutamine withdrawal (0 mM Gln), (D) in Panc1 cells. Dashed white line defines cell limits. White arrows indicate colocalisation of the indicated proteins (scale bar=10 µm). (E, F) PD of endogenous active ARF1 in WT/KO Panc1 cells on glutamine withdrawal. Quantification of active ARF1 pulled-down by GST (F, n=5). (G, H) PD of endogenous active ARF1 in WT, KO Panc1 or KO Panc1 cells re-expressing either tGFP-PI3K-C2γ WT or tGFP-PI3K-C2γ kD (kinase dead) on glutamine withdrawal for 2 hours. Representative Western blot images of active ARF1 PD assay probed with indicated antibodies (G). Quantification of active ARF1 pulled-down by GST (H, n=5). Data are shown as mean±SEM, ANOVA followed by Student's t-test (F) or Bonferroni's post hoc test (H). ANOVA, analysis of variance; PD, pull down; Tl, total lysate. **P<0.01.

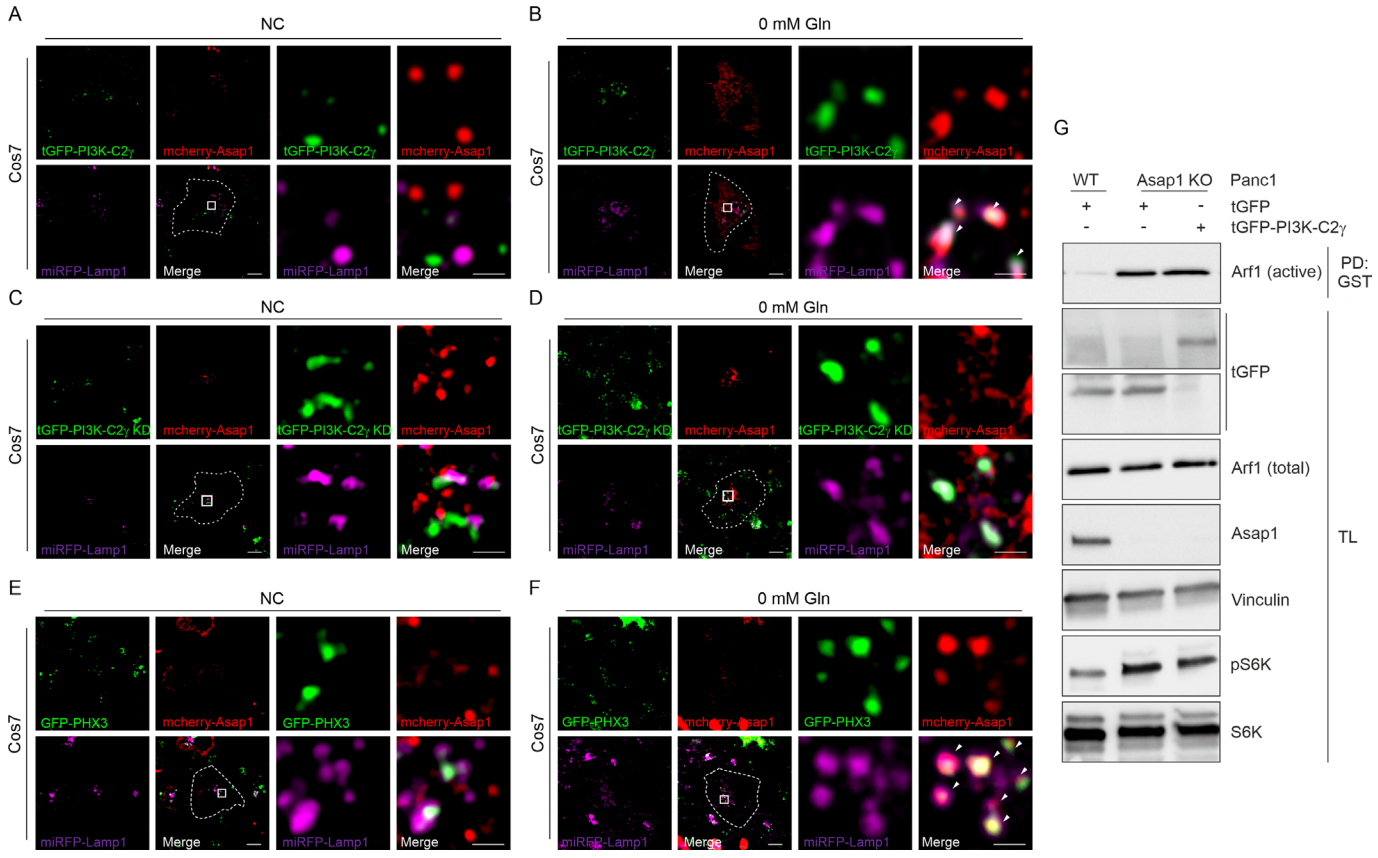

Figure 4 PI3K-C2γ-derived PI(3,4)P2 recruits Asap1 that inhibits Arf1 activity. (A, B) Localisation of PI3K-C2γ and Asap1 on Lamp1-positive lysosomes. Representative confocal images of tGFP-labelled PI3K-C2γ, mCherry-labelled ASAP1 and miRFP-labelled LAMP1 in normal culture conditions (NC, (A) or on glutamine withdrawal (0 mM Gln, (B) in Cos7 cells. Dashed white line defines cell limits. White arrows indicate colocalisation of the indicated proteins (scale bar=10 µm). (C, D) Localisation of PI3K-C2γ KD (kinase dead) and Asap1 on Lamp1-positive lysosomes. Representative confocal images of tGFP-labelled PI3K-C2γ KD, mCherry-labelled Asap1 and miRFP-labelled Lamp1 in normal culture conditions (NC, (C) or on glutamine withdrawal (0 mM Gln, (D) in Cos7 cells (scale bar=10 µm). (E, F) Localisation of PI(3,4)P2 and Asap1 on Lamp1-positive lysosomes. Representative confocal images of GFP-labelled PHX3, mCherry-labelled Asap1 and miRFP-labelled Lamp1 in normal culture conditions (NC), (E) or on glutamine withdrawal (0 mM Gln), (F) in Cos7 cells. Dashed white line defines cell limits. White arrows indicate colocalisation of the indicated proteins (scale bar=10 µm). (G) PD of endogenous active Arf1 and western blot analysis of mTORC1 activity probed with indicated antibodies in WT, Asap1 KO overexpressing tGFP or tGFP-PI3K-C2γ on glutamine withdrawal in Panc1 cells. mTORC1, mechanistic target of rapamycin complex 1; PD, pull down, TL, total lysate.

supplemental figure S6B,C). We found that re-expression of Asap1 R345L in Asap1 KO cells failed to deactivate Arf1 (online supplemental figure S6D), indicating that the PI(3,4)P2 generated by PI3K-C2γ on lysosomes is required for Asap1-mediated Arf1 inhibition in response to glutamine depletion.

Loss of PI3K-C2γ promotes glutamine metabolism rewiring

Next, we focused on PI3K-C2γ-dependent regulation of cell metabolism. We monitored the catabolic dependency of WT and KO cells using the Seahorse XF96 Mito Stress test to measure oxygen consumption rate in real time conditions. Analysis revealed that basal and maximal respiration were significantly lower in KO cells than WT controls (figure 5A–C and online supplemental figure S7A-C). Glutamine withdrawal for 24 hours dramatically decreased the respiratory capacity of WT cells while KO cells were marginally affected (figure 5A–C), indicating that the catabolic contribution of glutamine in KO cells is negligible. The higher spare respiratory capacity of KO cells (figure 5D and online supplemental figure S7D) was associated with enhanced glycolytic metabolism, as shown by increased glucose consumption and lactate release (figure 5E,F and online supplemental figure S7E,F). Therefore, we hypothesised that glutamine-auxotrophy of the PI3K-C2γ KO cells may be due to a potential non-energetic role of glutamine. Next, we measured the radioactive incorporation into lipids in cells that were cultured using the uniformly (U) radiolabeled ^{14}C-glutamine. Use of glutamine carbon units for lipid and protein synthesis was higher in KO cells than WT controls (figure 5G,H), thus indicating that glutamine carbon skeleton is consumed to support anabolic pathways.

Glutamine restriction abrogates growth of PI3K-C2γ-deficient cells

Subsequently, we explored the glutamine and glucose dependency of PI3K-C2γ-deficient tumours. While glucose was required for PDAC growth for both WT and KO cells (online supplemental figure S7G,H), most KO cells did not proliferate under glutamine withdrawal (figure 5I and online supplemental figure S7I). To validate the effect of glutamine on cell growth, WT and KO cells were cultured in presence or absence of glutamine. In normal growing conditions, KO cells exhibited significantly higher cell numbers than WT controls but glutamine withdrawal prominently hampered this growth, confirming that

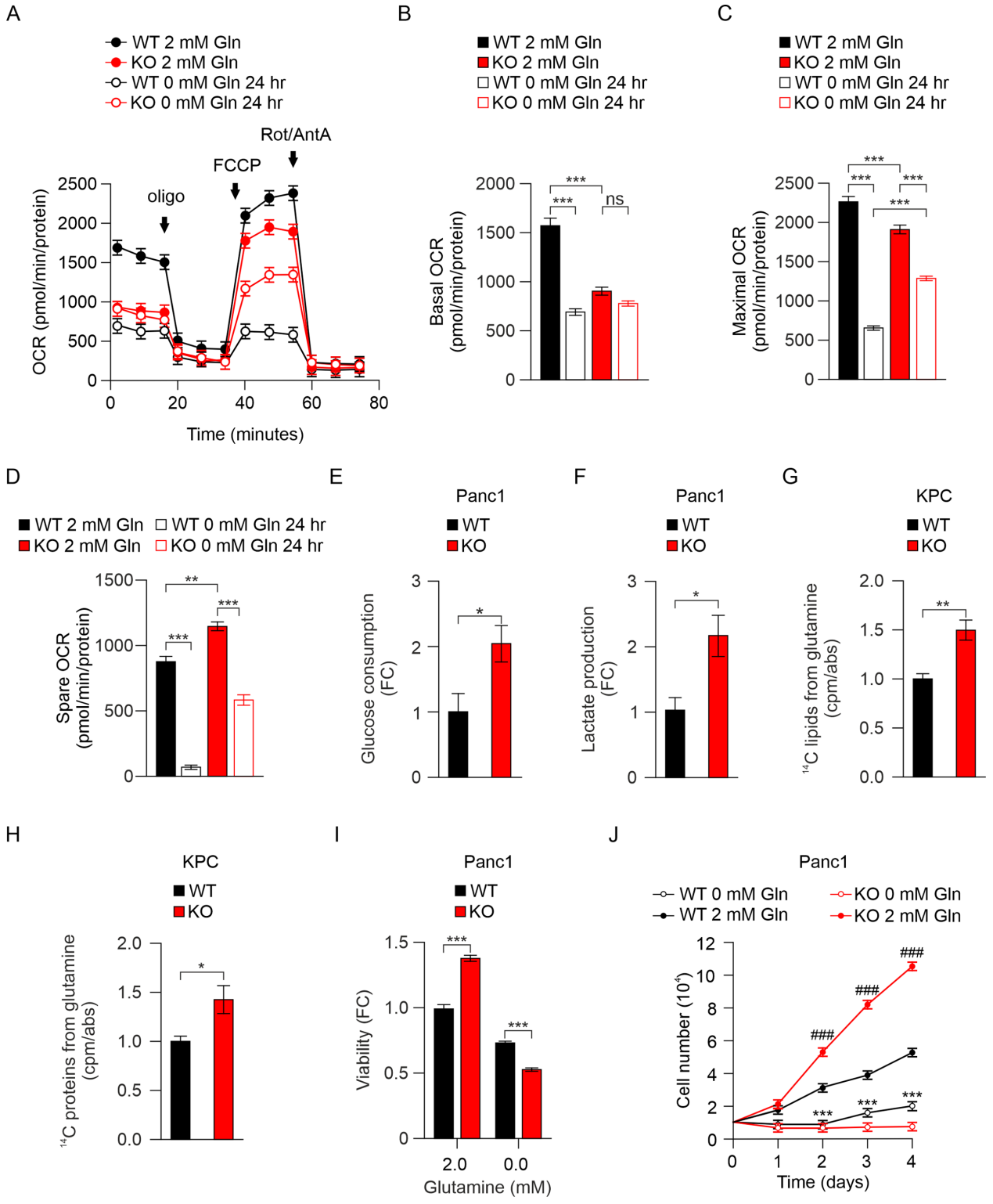

Figure 5 PI3K-C2γ loss induces metabolic rewiring towards the anabolic use of glutamine (A–D) seahorse XFe96 MITO stress test analysis and Oxygen Consumption Rate (OCR) was measured in real time in normal culture condition (2 mM Gln) or on 24 hours of glutamine withdrawal (0 mM Gln 24 hours) (n=3). Basal (B), maximal (C) and spare (D) OCR were measured and normalised on protein levels (n=3). Gln=glutamine, oligo=oligomycin, FCCP=carbonyl cyanide-4 (trifluoromethoxy) phenylhydrazone, Rot/AntA=rotenone/antimycin. (E) Quantification of glucose consumption in normal culture conditions (2 mM Gln) of WT/KO Panc1 cells (n=5). (F) Quantification of lactate production in normal culture conditions (2 mM Gln) of WT/KO Panc1 cells (n=5). (G, H) WT/KO KPC cells were cultured for 24 hours in a medium containing radioactive ^{14}C-glutamine. Lipids and proteins were extracted in parallel and radioactive signal was measured to monitor the amount of glutamine that is incorporated into lipids (G) and proteins (H). Each value was normalised on protein content (n=3). (I) Cell viability assay on WT/KO Panc1 cells at indicated glutamine concentrations after 24 hours (n=5). (J) Growth assay of WT/KO Panc1 cells in normal culture conditions (2 mM Gln) or on glutamine withdrawal (0 mM Gln) (n=5). #: KO 2 mM Gln vs KO 0 mM Gln); *: WT 0 mM Gln vs KO 0 mM Gln. Data are shown as mean±SEM, ANOVA followed by Bonferroni's post hoc test (B–D, I, J) or Student's t-test (E–H). ANOVA, analysis of variance. *P<0.05; **P<0.01; ***p<0.001; ***#<0.001.

KO cells are glutamine-addicted (figure 5J and online supplemental figure S7J). Next, we tested if different glutamine-metabolising pathways could rescue the growth deficit of KO cells on glutamine deprivation. Supplementation of BSA-conjugated palmitate, specifically rescued survival of KO cells while having no effect on WT controls (online supplemental figure S7K). On the contrary, addition of BSA alone did not improve cell survival either in KO or WT cells, thus indicating that only the exogenous supply of fatty acid precursors could bypass glutamine deprivation.

Loss of PI3K-C2γ sensitises pancreatic cancer cells to mTOR and GLS1 inhibitors

To pharmacologically replicate the sensitisation to glutamine depletion observed in the absence of PI3K-C2γ, we tested the effects of BPTES (Bis-2-(5-phenylacetamido-1,3,4-thiadiazol-2-yl) ethyl sulfide) and CB-839 (Telaglenastat), two potent inhibitors of glutaminase 1 (GLS1) activity.[36] Like glutamine starvation, administration of BPTES (online supplemental figure S8A,B) as well as CB-839 (figure 6A and online supplemental figure S8C,D) dose-dependently inhibited growth of KO cells, confirming that PI3K-C2γ-deficient cells are addicted to glutamine metabolism and that pharmacological inhibition of glutaminolysis can phenocopy the effect of glutamine restriction (figure 5I and online supplemental figure S7I). Treatment with GLS1 inhibitors increased the level of apoptosis in KO cells, as evidenced by caspase-3/7 activity levels (online supplemental figure S8E) without affecting the upstream phosphorylation status of S6K[37] (online supplemental figure S8F,G). Differently from WT, KO cells exhibited sustained AMPK phosphorylation in response to CB-839 administration (online supplemental figure S8H), indicating that interfering with glutamine metabolism strongly activates metabolic stress signalling. The administration of Everolimus (RAD001), a rapamycin analogue inhibiting mTORC1, decreased proliferation more effectively in KO cells than in WT controls, confirming the critical role of mTORC1 hyperactivation in PI3K-C2γ KO cells (figure 6A and online supplemental figure S8D). Likewise, either treatment with Everolimus in the presence of low glutamine (0.1 mM, online supplemental figure S8I) or combinatorial administration of Everolimus with CB-839 significantly hampered PI3K-C2γKO cells cell growth than WT controls, and appeared more effective than single treatments (figure 6A, online supplemental figure S8D and table S3).

To explore the antitumour potential of combination therapy in vivo, we first analysed a xenograft tumour model usingPanc1 cells. Administration of everolimus/BPTES alone or in combination was well tolerated and produced no apparent morbidity and/or mortality in mice. In vivo administration of Everolimus did not affect growth of WT Panc1 xenografts but, at 2.5 weeks of treatment, this drug appeared to effectively inhibit growth of PI3K-C2γ-deficient tumours ($p<0.001$; figure 6B). Likewise, BPTES inhibited cancer growth more strongly in KO than in WT Panc1 xenografts ($p<0.05$; figure 6B). Furthermore, the combination of Everolimus and BPTES resulted in a stronger anticancer response, that was again more pronounced in KO than in WT xenografts ($p<0.001$; figure 6B). Consistently, PI3K-C2γ deleted tumours treated with combination therapy exhibited reduced levels of PCNA staining compared with WT and to untreated KO controls (figure 6C). In line with in vitro data, Everolimus but not BPTES treatment reduced S6 phosphorylation in tumour samples (figure 6C). Similar results were also obtained in a second mouse model where KPC murine cells were subcutaneously injected in syngeneic mice (figure 6D and S9A). Finally, efficacy of the everolimus/BPTES combination was tested in KPC mouse model (online supplemental figure S9B-D). T_{2w} MRI showed the presence of ascites and pancreatic tumours, that appeared as heterogeneous hyperintense nodules in all groups (online supplemental figure S9B). The combo therapy delayed progression, improved tumour edge definition, and reduced abdominal spread (online supplemental figure S9B). Accordingly, the combo treatment significantly increased survival of KO mice (100% vs 80% survival at 8 weeks of combo and vehicle-treated KO mice, respectively; $n=5$ per group, $p=0.01$ by log-rank Mantel-Cox test, online supplemental figure S9C). In line with previous results, PCNA was less intense in KPC KO tumours treated with the combo than in treated WT tumour samples or untreated KO controls (online supplemental figure S9D). Collectively, these results indicated that the combination therapy is more effective in the PI3K-C2γ KO genetic background, demonstrating that loss of PI3K-C2γ sensitises pancreatic cancer cells and tumours to mTOR and GLS1 inhibitors (online supplemental figure S10).

DISCUSSION

Pancreatic cancer is one the most aggressive tumours and currently available therapies are only minimally effective in treating this disease. The metabolism of pancreatic cancer is adapted to support tumour growth in its nutrient-deprived environment.[2]

A central integrator of cell growth and nutrient availability is the mTOR pathway, which drives metabolic reprogramming to support the biosynthetic needs of cancer cells.[38] While mTOR is activated by class I PI3K, our results indicated that class II PI3K-C2γ acts as a negative regulator of mTOR signalling, in line with previous findings.[13] The fact that class II PI3Ks work differently from class I enzymes is consolidating and, while the role of class I PI3K as oncogenes is well established, class II PI3K are emerging as tumour suppressors controlling cell division[39] as well as other cellular functions linked to cell growth.[12 16 40] In this study, we demonstrated that the loss of PI3K-C2γ in mice confers a growth advantage to pancreatic cancer cells, correlating with hyperactivation of the mTORC1 signalling and metabolic shift towards glutamine dependency. In agreement, increased phosphorylation of the S6 correlated with decreased expression of PI3K-C2γ in a cohort of patients. Although only a trend could be evidenced for another mTORC1 effector, like 4EBP1, this potential inconsistency might be attributed not only to the relatively small number of samples analysed ($n=37$) but also to the ability of 4EBP1 to be regulated by multiple pathways other than that of mTORC1.[41] In further support to our hypothesis, reduced expression of PI3K-C2γ correlated with poor prognosis and a more aggressive phenotype, not only indicating a function of PI3K-C2γ as a tumour suppressor in PDAC but also suggesting a role of this protein as a potential prognostic biomarker.

At the molecular level, our results demonstrated that PI3K-C2γ restrains mTORC1 activity at the lysosome through the production of a restricted pool of PI(3,4)P2 in response to glutamine withdrawal. Various effectors can relay inhibitory signals to restrain mTORC1 activity,[11 30] including the class II PI3K-C2β isoform.[13] Nevertheless, while PI3K-C2β acts on growth factor deprivation,[13 14] our results showed that PI3K-C2γ selectively responds to glutamine starvation. In particular, glutamine deprivation couples PI3K-C2γ activity to mTORC1 signalling, leading to the accumulation of a PI3K-C2γ-generated pool of PI(3,4)P2 that in turn reduces S6K phosphorylation. How PI3K-C2γ translocation to lysosomes is regulated by glutamine availability is at

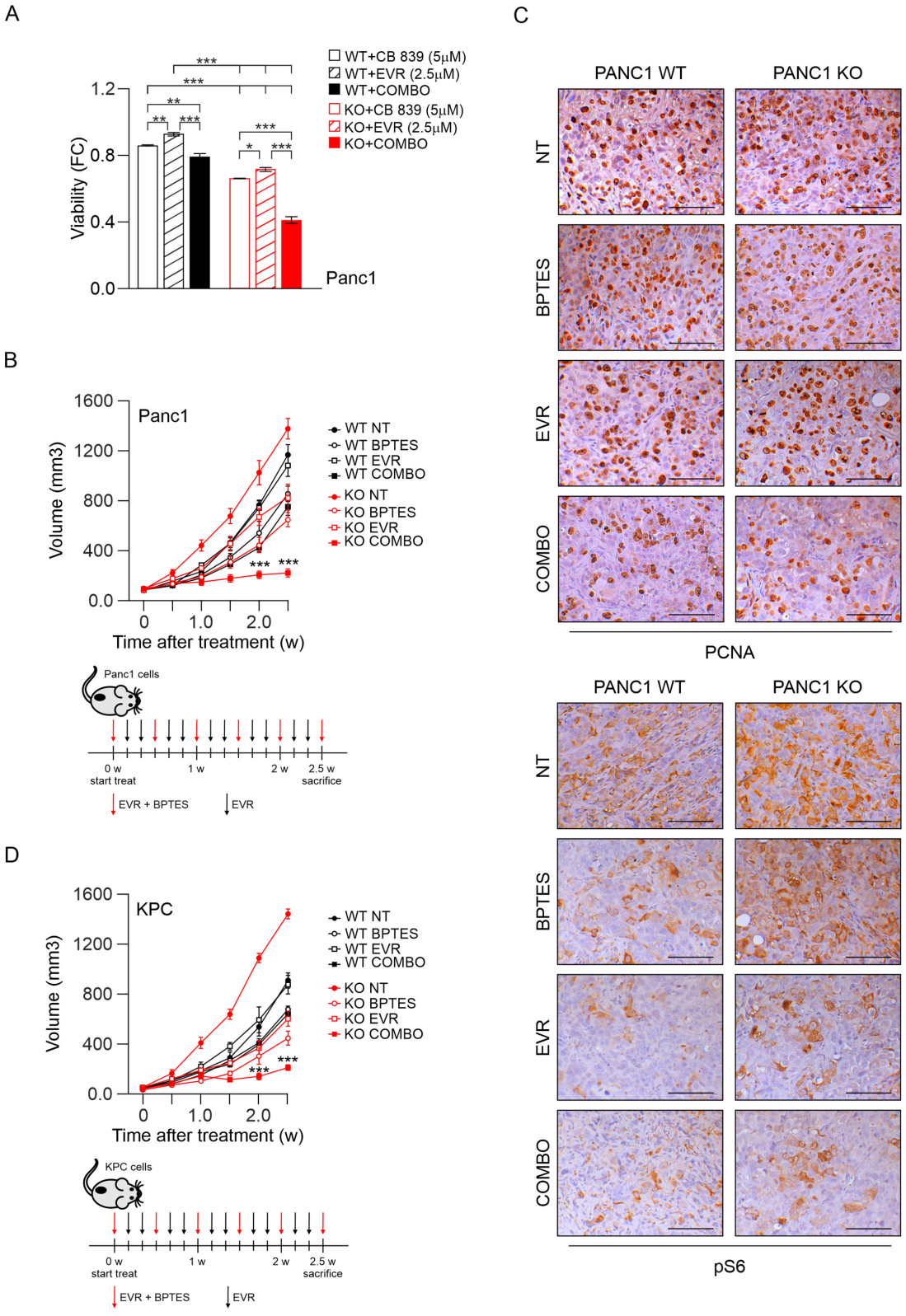

Figure 6 PI3K-C2γ loss sensitises to glutaminase inhibitors in xenograft models. (A) Cell viability assay on WT/KO Panc1 cells after 48 hours of treatment with CB 839 (5 µM), everolimus (2.5 µM) or combination of the two drugs (Combo, n=6). (B) quantification of xenograft tumour growth arising from subcutaneously injected WT/KO Panc1 cells. Mice were treated for 2.5 weeks (w) with intraperitoneal injections of vehicle (NT), BPTES, everolimus (EVR) or combination (COMBO) of the two drugs (n=6). Schematic representation of drugs administration (bottom panels). (C) IHC assessment of the level of PCNA (top) and pS6 (bottom) in tumours taken from mice injected with WT/KO Panc1 cells treated with vehicle (NT), BPTES, everolimus (EVR) or combination (COMBO) of the two drugs for 2.5 weeks. (D) quantification of xenograft tumour growth arising from subcutaneously injected WT/KO KPC cells. Mice were treated for 2.5 weeks (w) with intraperitoneal injections of vehicle (NT), BPTES, everolimus (EVR) or combination (COMBO) of the two drugs (n=6). Schematic representation of drugs administration (bottom panels). Data are shown as mean±SEM, ANOVA followed by Bonferroni's post hoc test. ANOVA, analysis of variance. *P<0.05; **P<0.01; ***p<0.001.

this stage unclear and the focus of future studies. Nonetheless, our findings are in line with phospholipids playing a key role in the control of metabolic responses through the docking of PH-domain containing proteins.[15 42]

In agreement with the established role of mTORC1 in promoting anabolic reactions,[30] our results showed that the loss of PI3K-C2γ rewires glutamine metabolism to support lipid and protein biosynthesis, sustaining the higher growth rate of KO cells. However, failure of PI3K-C2γ-deficient tumours to limit mTORC1 signalling and anabolic processes leading to glutamine addiction can turn detrimental when glutamine levels decline. Our findings showed that cells lacking PI3K-C2γ become auxotrophic for glutamine, a condition that characterises several glutamine-dependent tumours.[7] In PI3K-C2γ-deficient tumours, glutamine consumption thus exceeded its biosynthesis, leading to synthetic lethality between loss of PI3K-C2γ and glutamine starvation. Therefore, the inability of PI3K-C2γ KO tumours to curtail cell growth in nutrient limiting-condition results in a 'metabolic catastrophe', a metabolic state in which high anabolic demand is contrasted by insufficient energy production.[43] Based on these findings, targeting the metabolic phenotype of PI3K-C2γ-deficient tumours can be further exploited by specific therapeutic strategies in pancreatic cancer.

This critical role of glutamine in pancreatic cancer has fostered the development of pharmacological strategies to target glutamine utilisation.[4] A crucial step in the metabolism of glutamine that supports cancer growth is its conversion to glutamate by the enzyme glutaminase (GLS1). Inhibitors of GLS1, such as CB-839, showed clinical benefits in PDAC patients[44] (NCT03263429). Moreover, a combination therapy of CB-839 with Everolimus is currently undergoing clinical trials in patients with advanced solid tumours (NCT02071862), indicating that the drug combination is well tolerated.[45] Nevertheless, biomarkers are needed to identify different sub-populations of patients who can receive highest benefit from glutaminase inhibitors.

Our findings provide a rationale for targeting glutamine metabolism in combination with mTOR inhibitors in tumours with reduced expression of PI3K-C2γ and hyperactive mTOR signalling. Furthermore, our study suggests that targeting PI3K-C2γ or its downstream effectors may unveil metabolic vulnerabilities that can be further exploited for pancreatic cancer therapy, if cotreated with mTOR inhibitors.

Author affiliations
[1]Department of Molecular Biotechnology and Health Sciences, University of Turin, Torino, Italy
[2]Department of Biomedical, Experimental and Clinical Sciences, University of Florence, Firenze, Italy
[3]Department of Innovative Technologies in Medicine and Dentistry, Center for Advanced Studies and Technology (CAST), University "G. d'Annunzio", Chieti, Italy, Chieti, Italy
[4]Department of Medical Oncology, Cancer Center Amsterdam, Amsterdam University Medical Centers, VU University, De Boelelaan 1117, 1081, HV, Amsterdam, The Netherlands
[5]Cancer Pharmacology Lab, Fondazione Pisana per la Scienza, Pisa, Italy
[6]ARC-Net Research Centre, University of Verona, Verona, Italy
[7]Department of Diagnostics and Public Health, University of Verona, Verona, Italy

Twitter Silvia Andreani @SilviaAndreani7

Acknowledgements We thank Prof. Andrea Graziani, Dr. Alessio Menga, Dr. Carlo Cosimo Campa, Prof. Vincenzo Calautti, Prof. Riccardo Taulli and Prof. Chiara Ambrogio for critically reading the manuscript and useful discussion. We acknowledge the Open Lab of Advanced Microscopy (OLMA) at the Molecular Biotechnology Centre (MBC) for support and Euro-BioImaging (www.eurobioimaging.eu) for providing access to imaging technologies and services via the MultiModal Molecular Imaging Italian Node (Torino, Italy). The data of the PanCuRx cohort used in this study were generated with the support of the Ontario Institute for Cancer Research through funding provided by the Government of Ontario.

Contributors Conceptualisation: MCDS, EH, MM; Methodology: MCDS, LG, AC, JPM, FG, EDG, RL, GS, SA, PD, CV, EG, VC, PEP, AM, EH and MM; Data curation: PD, CV and VCValidation: MCDS, EH and MM; Formal Analysis: MCDS, LG, AC, ER, JPM, FG, EM, NL, MB, RL, GS, SA, PD, CV, EG, VC, AM and MM. Investigation: MCDS, LG, AC, ER, JPM, FG, EM, NL, MB, RL, GS, SA, PD, CV, EG, VC, AM and MM. Resources: PDAC, FN, CV, EG, VC, AS; Writing-original draft preparation, MCDS, EH and MM; Visualisation: MCDS, EH, MM; Supervision: VC, AS, PEP, AM, EH, MM; Project Administration: MCDS, EH, MM; Funding Acquisition: EH, MM; Guarantor: MCDS, EH, MM.

Funding MCDS and JPM are supported by Fondazione Italiana per la Ricerca sul Cancro/Associazione Italiana Ricerca sul Cancro (FIRC/AIRC) fellowships (22 248 and 22558). FG is supported by Fondazione Pezcoller/SIC-Patrizia Coser. MM is supported by Worldwide Cancer Research grant (WWCR, 20–0033). EH is supported by AIRC (21875), MIUR (Ministero Università Ricerca, PRIN 2017) and Leducq Transatlantic Network of Excellence (19CVD02). EG is supported by AIRC (IG24444) and Dutch Cancer Society (KWF-11957). PD is supported by Fondazione Nadia Valsecchi Onlus. VC and AS are supported by AIRC (18 718 and 12182). AS is also supported by Italian Ministry of Health (FIMPDACUP_J38D19000690001). PEP is supported by AIRC (MFAG 2018 - ID. 21564). MB is supported by Fondazione Pezcoller/SIC Prof. ssa De Gasperi Ronc. AM is supported by AIRC and Fondazione Cassa di Risparmio di Firenze (IG22941 and MultiUser19515). FN is supported by AIRC (IG19931) and Fondazione Ricerca Molinette Onlus (Fondo CD38, Fondo Ursula and Giorgio Cytron). The data presented in the current study were in part generated using the equipment of the Facility di Medicina Molecolare, funded by 'Ministero dell'Istruzione dell'Università e della Ricerca-Bando Dipartimenti di Eccellenza 2018–2022' (AM).

Competing interests EH is a founder of Kither Biotech, a company involved in the development of PI3K inhibitors. The authors declare no potential conflicts of interest.

Patient and public involvement Patients and/or the public were not involved in the design, or conduct, or reporting, or dissemination plans of this research.

Patient consent for publication Not applicable.

Ethics approval Ethics approval number 1885 from the Integrated University Hospital Trust (AOUI) Ethics Committee (Comitato Etico Azienda Ospedaliera Universitaria Integrata) was approved in their meeting of 17 November 2010 and documented by the ethics committee 52070/CE on 22 November 2010 and formalised by the Health Director of the AOUI on the order of the General Manager with protocol 52 438 on 23 November 2010.The study protocol was approved by the local Ethics Committee at University Hospital of Pisa, Italy (Comitato di Bioetica, Azienda Ospedaliero-Universitaria Pisana, protocol number: 3909, July third, 2013).

Provenance and peer review Not commissioned; externally peer reviewed.

Data availability statement Data are available in a public, open access repository. Data are available on reasonable request. All data relevant to the study are included in the article or uploaded as online supplemental information. Not applicable.

ORCID iDs
Luca Gozzelino http://orcid.org/0000-0001-9578-647X
Jean Piero Margaria http://orcid.org/0000-0002-2435-7499
Gianluca Sala http://orcid.org/0000-0002-4494-915X
Paola Cappello http://orcid.org/0000-0002-5321-7794
Vincenzo Corbo http://orcid.org/0000-0002-6340-8009
Aldo Scarpa http://orcid.org/0000-0003-1678-739X
Miriam Martini http://orcid.org/0000-0002-4262-946X

REFERENCES

1 Siegel RL, Miller KD, Jemal A. Cancer statistics. In: *CA: a cancer Journal for clinicians 2020*. , 2020: 70, 7–30.
2 Perera RM, Bardeesy N. Pancreatic cancer metabolism: breaking it down to build it back up. *Cancer Discov* 2015;5:1247–61.

3 Derle A, De Santis MC, Gozzelino L, *et al*. The role of metabolic adaptation to nutrient stress in pancreatic cancer. *Cell Stress* 2018;2:332–9.
4 Son J, Lyssiotis CA, Ying H, *et al*. Glutamine supports pancreatic cancer growth through a KRAS-regulated metabolic pathway. *Nature* 2013;496:101–5.
5 Biancur DE, Paulo JA, Małachowska B, *et al*. Compensatory metabolic networks in pancreatic cancers upon perturbation of glutamine metabolism. *Nat Commun* 2017;8:15965.
6 DeBerardinis RJ, Cheng T. Q's next: the diverse functions of glutamine in metabolism, cell biology and cancer. *Oncogene* 2010;29:313–24.
7 Altman BJ, Stine ZE, Dang CV. From Krebs to clinic: glutamine metabolism to cancer therapy. *Nat Rev Cancer* 2016;16:619–34.
8 Hassan Z, Schneeweis C, Wirth M, *et al*. MTOR inhibitor-based combination therapies for pancreatic cancer. *Br J Cancer* 2018;118:366–77.
9 Wolpin BM, Hezel AF, Abrams T, *et al*. Oral mTOR inhibitor everolimus in patients with gemcitabine-refractory metastatic pancreatic cancer. *J Clin Oncol* 2009;27:193–8.
10 Kong B, Wu W, Cheng T, *et al*. A subset of metastatic pancreatic ductal adenocarcinomas depends quantitatively on oncogenic Kras/Mek/Erk-induced hyperactive mTOR signalling. *Gut* 2016;65:647–57.
11 Liu GY, Sabatini DM. mTOR at the nexus of nutrition, growth, ageing and disease. *Nat Rev Mol Cell Biol* 2020;21:183–203.
12 Bilanges B, Posor Y, Vanhaesebroeck B. PI3K isoforms in cell signalling and vesicle trafficking. *Nat Rev Mol Cell Biol* 2019;20:515–34.
13 Marat AL, Wallroth A, Lo W-T, *et al*. Mtorc1 activity repression by late endosomal phosphatidylinositol 3,4-bisphosphate. *Science* 2017;356:968–72.
14 Wallroth A, Koch PA, Marat AL, *et al*. Protein kinase N controls a lysosomal lipid switch to facilitate nutrient signalling via mTORC1. *Nat Cell Biol* 2019;21:1093–101.
15 Gozzelino L, De Santis MC, Gulluni F, *et al*. PI(3,4)P2 Signaling in Cancer and Metabolism. *Front Oncol* 2020;10:360.
16 Gulluni F, De Santis MC, Margaria JP, *et al*. Class II PI3K functions in cell biology and disease. *Trends Cell Biol* 2019;29:339–59.
17 Braccini L, Ciraolo E, Campa CC, *et al*. PI3K-C2gamma is a Rab5 effector selectively controlling endosomal Akt2 activation downstream of insulin signalling. *Nat Commun* 2015;6:7400.
18 Hingorani SR, Wang L, Multani AS, *et al*. Trp53R172H and KrasG12D cooperate to promote chromosomal instability and widely metastatic pancreatic ductal adenocarcinoma in mice. *Cancer Cell* 2005;7:469–83.
19 Hruban RH, Adsay NV, Albores-Saavedra J, *et al*. Pathology of genetically engineered mouse models of pancreatic exocrine cancer: consensus report and recommendations. *Cancer Res* 2006;66:95–106.
20 Cerami E, Gao J, Dogrusoz U, *et al*. The cBio cancer genomics portal: an open platform for exploring multidimensional cancer genomics data. *Cancer Discov* 2012;2:401–4.
21 Gao J, Aksoy BA, Dogrusoz U, *et al*. Integrative analysis of complex cancer genomics and clinical profiles using the cBioPortal. *Sci Signal* 2013;6:pl1.
22 Peng J, Sun B-F, Chen C-Y, *et al*. Single-Cell RNA-seq highlights intra-tumoral heterogeneity and malignant progression in pancreatic ductal adenocarcinoma. *Cell Res* 2019;29:725–38.
23 Lin W, Noel P, Borazanci EH, *et al*. Single-Cell transcriptome analysis of tumor and stromal compartments of pancreatic ductal adenocarcinoma primary tumors and metastatic lesions. *Genome Med* 2020;12:80.
24 Chan-Seng-Yue M, Kim JC, Wilson GW, *et al*. Transcription phenotypes of pancreatic cancer are driven by genomic events during tumor evolution. *Nat Genet* 2020;52:231–40.
25 Steele NG, Carpenter ES, Kemp SB, *et al*. Multimodal mapping of the tumor and peripheral blood immune landscape in human pancreatic cancer. *Nat Cancer* 2020;1:1097–112.
26 Moffitt RA, Marayati R, Flate EL, *et al*. Virtual microdissection identifies distinct tumor- and stroma-specific subtypes of pancreatic ductal adenocarcinoma. *Nat Genet* 2015;47:1168–78.
27 Bailey P, Chang DK, Nones K, *et al*. Genomic analyses identify molecular subtypes of pancreatic cancer. *Nature* 2016;531:47–52.
28 Cancer Genome Atlas Research Network. Electronic address: andrew_aguirre@dfci.harvard.edu, Cancer Genome Atlas Research Network. Integrated genomic characterization of pancreatic ductal adenocarcinoma. *Cancer Cell* 2017;32:e13:185–203.
29 Kim J, Guan K-L. mTOR as a central hub of nutrient signalling and cell growth. *Nat Cell Biol* 2019;21:63–71.
30 Saxton RA, Sabatini DM. mTOR signaling in growth, metabolism, and disease. *Cell* 2017;168:960–76.
31 Jewell JL, Kim YC, Russell RC, *et al*. Metabolism. Differential regulation of mTORC1 by leucine and glutamine. *Science* 2015;347:194–8.
32 Meng D, Yang Q, Wang H, *et al*. Glutamine and asparagine activate mTORC1 independently of RAG GTPases. *J Biol Chem* 2020;295:2890–9.
33 Roy NS, Jian X, Soubias O, *et al*. Interaction of the N terminus of ADP-ribosylation factor with the pH domain of the GTPase-activating protein ASAP1 requires phosphatidylinositol 4,5-bisphosphate. *J Biol Chem* 2019;294:17354–70.
34 Kam JL, Miura K, Jackson TR, *et al*. Phosphoinositide-dependent activation of the ADP-ribosylation factor GTPase-activating protein ASAP1. Evidence for the pleckstrin homology domain functioning as an allosteric site. *J Biol Chem* 2000;275:9653–63.
35 Wullschleger S, Wasserman DH, Gray A, *et al*. Role of TAPP1 and TAPP2 adaptor binding to PtdIns(3,4)P2 in regulating insulin sensitivity defined by knock-in analysis. *Biochem J* 2011;434:265–74.
36 Li L, Meng Y, Li Z, *et al*. Discovery and development of small molecule modulators targeting glutamine metabolism. *Eur J Med Chem* 2019;163:215–42.
37 Csibi A, Lee G, Yoon S-O, *et al*. The mTORC1/S6K1 pathway regulates glutamine metabolism through the eIF4B-dependent control of c-myc translation. *Curr Biol* 2014;24:2274–80.
38 De Santis MC, Porporato PE, Martini M, *et al*. Signaling pathways regulating redox balance in cancer metabolism. *Front Oncol* 2018;8:126.
39 Gulluni F, Martini M, De Santis MC, *et al*. Mitotic spindle assembly and genomic stability in breast cancer require PI3K-C2α scaffolding function. *Cancer Cell* 2017;32:444–59.
40 Gulluni F, Prever L, Li H, *et al*. PI(3,4)P2-mediated cytokinetic abscission prevents early senescence and cataract formation. *Science* 2021;374:eabk0410.
41 Qin X, Jiang B, Zhang Y. 4E-BP1, a multifactor regulated multifunctional protein. *Cell Cycle* 2016;15:781–6.
42 Kavran JM, Klein DE, Lee A, *et al*. Specificity and promiscuity in phosphoinositide binding by pleckstrin homology domains. *J Biol Chem* 1998;273:30497–508.
43 Pavlova NN, Thompson CB. The emerging hallmarks of cancer metabolism. *Cell Metab* 2016;23:27–47.
44 Mukhopadhyay S, Goswami D, Adiseshaiah PP, *et al*. Undermining glutaminolysis bolsters chemotherapy while Nrf2 promotes chemoresistance in KRas-driven pancreatic cancers. *Cancer Res* 2020;80:1630–43.
45 Shen Y-A, Chen C-L, Huang Y-H, *et al*. Inhibition of glutaminolysis in combination with other therapies to improve cancer treatment. *Curr Opin Chem Biol* 2021;62:64–81.

SUPPLEMENTAL MATERIAL

Supplemental Tables

Table S1. Distribution of PI3K-C2γ expression in patients cohorts

	PI3K-C2γ expression			
	IHC score <1	IHC score ≥1	Row Totals	p-value*
Cohort 1	28 (38%)	45 (62%)	73	0.099
Cohort 2	17 (22.4%)	59 (77.6%)	76	
Cohort 3	15 (33.3%)	30 (66.7%)	45	
Column totals	60	134	194	

*chi-square test

Table S2. Biochemical analysis of Pik3c2g$^{+/+}$ (WT) and Pik3c2g$^{-/-}$ (KO) mice.

		WT		KO	
		mean	sd	mean	sd
liver function	ALT (U/L)	103	23	107	24,04163
	GGT (U/L)	0	0	0	0
	TP (g/dl)	4,9	0,7	4,6	0,565685
	ALB (g/dl)	2,05	0,15	2,05	0,212132
	TBIL (mg/dL)	0,1	1,7E-17	0,15	0,070711
	GLOB (g/dL)	2,85	0,55	2,55	0,353553
	ALB/GLOB	1,05	0,15	1,2	0,565685
	ALKP (U/L)	125	31	134	56,56854
renal function	CREA (mg/dL)	0,1	1,7E-17	0,1	0
	BUN (mg/dL)	24,5	6,5	22	8,485281
	PHOS (mg/dL)	7,5	0,9	7,6	0,777817
	Ca (mg/dL)	7,95	0,95	8,5	1,272792
pancreatic function	AMYL (U/L)	1912,5	137,5	1654	209,3036
	LIPA (U/L)	695	25	770	50,91169

ALT=alanine aminotransferase, GGT=g-glutamyl transferase, TP=total protein, ALB=albumin, TBIL=total bilirubin, GLOB=globulins, ALB/GLOB=albumin/globulin, ALKP=alkaline phosphatase, CREA=creatinine, BUN=blood urea nitrogen, PHOS=inorganic phosphate, Ca=calcium, AMYL=amylase, LIPA=lipase.

Statistical analysis did not show significant differences in all the parameters measured (P>0.05, n=3 mice, sd=standard deviation).

Table S3. Combination Index (C.I.) for CB 839 (CB) and Everolimus (EVR) treatment

C.I.	CB (uM)	EVR (uM)	CB (uM)	EVR (uM)	CB (uM)	EVR (uM)	CB (uM)	EVR (uM)	CB (uM)	EVR (uM)
	2.5	1.25	5	2.5	10	5	20	10	40	20
WT	0.95		0.83		0.71		0.82		0.94	
KO	0.88		0.28		0.36		0.49		0.75	

Supplemental Figure legends

Figure S1.

PI3K-C2γ loss decreases survival in patients and accelerates tumor development in KPC mice

(A) Gene expression analysis (scRNA-Seq) performed in PDAC datasets.

(B) Comparison of *PIK3C2G* expression in TCGA or ICGC PC cases stratified by Moffitt subtypes (basal-like and classical). Results are shown as mean ± SD (p=0.035 and p=0.013 by Wilcoxon rank-sum test).

(C) Correlation analysis of PI3K-C2γ and GATA6 expression in TCGA (n=148) or ICGC (n=95) PDAC datasets (p=0.014 and p<0.01 by Wilcoxon rank-sum test).

(D) PI3K-C2γ antibody validation by IHC on *Pik3c2g*$^{+/+}$ and *Pik3c2g*$^{-/-}$ mice (scale bar=100 μm).

(E) IHC assessment of the level of PI3K-C2γ expression in moderately and poorly differentiated PDACs from cohort #1 (scale bar=100 μm, n=73).

(F-G) Kaplan-Meier survival analysis showing the relationship between PI3K-C2γ expression (high: score ≥1 or low: score < 1) and overall survival (OS) (n= 76, p=0.035 by Mantel-Cox log-rank test) or progression free survival (PFS, n=76, p=0.318 by Mantel-Cox log-rank test) in cohort #2 of PDAC patients.

(H) Circulating levels of the pancreatic enzyme lipase in WT and KO mice fed with normal chow (CTRL) or metabolically challenging diet (HFD, n=4 mice).

(I-J) Assessment of number and grade of PanIN lesions in WT/KO KPC mice. Representative IHC staining for PI3K-C2γ (I) and quantification of the number of lesions per field (J). Arrows indicate PanIN lesions, asterisks (*) indicate normal acini, hashtags (#) indicates PDAC (scale bar=100 μm, n ≥ 6).

(K) Measurement of blood glucose levels of 1 month (1m) or 2 months (2m) old WT/KO KPC mice (n=3).

Data are shown as mean ± SEM, ANOVA followed by Bonferroni's post hoc test, otherwise indicated.

Figure S2.

PI3K-C2γ loss increases metastatization in KPC mice and accelerates PC cells growth

(A) Quantification of liver and lung macrometastasis in WT/KO KPC mice (n=6 mice, 3 sections per mice).

(B) IHC assessment of PI3K-C2γ expression levels of primary tumor cell lines derived from KPC WT/KO mice.

(C) Quantification of tumor growth arising from subcutaneously injected WT/KO KPC cell lines in syngeneic mice (n=6).

(D) Liver and lung macrometastasis count arising from subcutaneously injected WT/KO KPC cells in syngeneic mice (n=6 mice, 3 sections per mice).

(E) Relative invasive ability of WT/KO KPC cells (n=5).

(F-H) Real time qPCR analysis for *PIK3C2G* expression levels in Capan1 (F), MiaPaca2 (G) and Panc1 (H) after Crispr/Cas9 *PIK3C2G* editing and single cell selection (n=5).

(I) IHC assessment of PI3K-C2γ expression levels in WT/KO Panc1 cells (scale bar=100 μm)

(J-K) Cell growth assay of WT/KO Capan1 (J) and MiaPaca2 (K) cells (n=5).

(L-M) Western blot analysis of Erk phosphorylation in WT/KO KPC (L) and Panc1 (M) cells. Representative western blot images of whole-cell lysates probed with indicated antibodies.

Data are shown as mean ± SEM, Student t test (E-H) or ANOVA followed by Bonferroni's post hoc test (A,C,D,J,K).

Figure S3.

PI3K-C2γ loss induces mTORC1 hyperactivation upon glutamine deprivation

(A) IHC assessment of the level of expression of PCNA and pS6 in tumors arising from subcutaneously injected WT/KO Panc1 or KPC cells in syngeneic mice (scale bar=100 μm).

(B) Western blot analysis of mTORC1 activity in WT/KO KPC cells upon glutamine withdrawal (0 mM Gln) for 2 hours. Representative western blot images of whole-cell lysates probed with indicated antibodies.

(C-D) Western blot analysis (C) and quantifications (D) of mTORC1 activity in WT/KO Panc1 cells in normal culture condition (NC), upon FBS deprivation (-FBS) or glutamine withdrawal for 2 hours (-Gln, n=4).

(E) IHC assessment and quantification of the level of p4EBP1 expression in PDAC patients expressing high (score ≥ 1) or low (score <1) PI3K-C2γ levels from cohort #3 (n=45, Spearman's correlation analysis, scale bar=100 μm).

(F) IHC assessment of the level of pS6 expression in moderately-well/moderately and poorly differentiated PDACs from cohort #3 (scale bar=100 μm, n=45).

Data are shown as mean ± SEM, ANOVA followed by Bonferroni's post hoc test, otherwise indicated.

Figure S4.

AKT signaling is not affected by PI3K-C2γ loss

(A-B) Western blot analysis of Akt phosphorylation in WT/KO KPC cells transfected with tGFP, tGFP-labeled PI3K-C2γ WT or tGFP-labeled PI3K-C2γ KD in serum starved culture conditions (-INS, A) and stimulated with insulin where indicated (+INS, A) or upon glutamine deprivation (0 mM Gln, B) for 2 hours. Representative western blot images of whole-cell lysates probed with indicated antibodies.

(C-D) Western blot analysis of Akt phosphorylation in WT/KO Panc1 cells transfected with tGFP, tGFP-labeled PI3K-C2γ WT or tGFP-labeled PI3K-C2γ KD in serum starved culture conditions (-INS, C) and stimulated with insulin where indicated (+INS, C) or upon glutamine deprivation (0 mM Gln, D) for 2 hours. Representative western blot images of whole-cell lysates probed with indicated antibodies.

(E-F) mTOR kinase assay performed on WT/KO Panc1 cells upon 2 hrs glutamine starvation. Raptor or control IgG was immunoprecipitated (IP) from WT/KO Panc1 cells and analyzed for mTORC1 activity. Representative western blot images of IP and whole-cell lysates probed with indicated antibodies (E) and quantification of pS6K/mTOR ratio (F, n=5).

(G) ELISA quantification of whole-cell PI(3,4)P2 levels in WT/KO KPC cells upon glutamine withdrawal (0 mM Gln) for 2 hours (n>3).

(H-I) Localization of mTOR on Lamp1 positive vesicles in WT/KO Panc1 cells upon glutamine deprivation. Quantification (n>110 cells, H) and representative immunofluorescence images of mTOR (green), Lamp1 (magenta) and nuclei (blue) stainings (scale bar=5 μm, I).

Data are shown as mean ± SEM, by Student t test.

Figure S5.

PI3K-C2γ-derived PtdIns(3,4)P2 inhibits Arf1 activity

(A-B) Localization of PI3K-C2γ on Lamp1-positive lysosomes. Representative confocal images of tGFP-labeled PI3K-C2γ and miRFP-labeled Lamp1 in normal culture conditions (NC) and upon glutamine withdrawal (0 mM Gln) for 2 hours in Cos7 cells (A) (scale bar=10 μm). Quantification of PI3K-C2γ localization on Lamp1-positive endosomes (B). The ratio of PI3K-C2γ-Lamp1-positive lysosomes was adjusted by the mean number of Lamp1-positive spots in every experimental condition. Dashed white line defines cell limits. White arrows indicate co-localization of the indicated proteins (scale bar=10 μm, n=18).

(C-D) Localization of PI3K-C2γ and PI(3,4)P2 on Lamp1-positive lysosomes. Representative confocal images of tGFP-labeled PI3K-C2γ, mcherry-labeled PHX3 and miRFP-labeled Lamp1 in normal culture conditions (NC, C) or upon glutamine withdrawal (0 mM Gln, D) in Cos7 cells. Dashed white line defines cell limits. White arrows indicate co-localization of the indicated proteins (scale bar=10 μm).

(E) Quantification of the number of lysosomes positive for PI(3,4)P2 in Panc1 cells in normal culture conditions (NC) and upon glutamine withdrawal (0 mM Gln) for 2 hours (n=5).

(F) Quantification of the number of lysosomes positive for PI3K-C2γ and PI(3,4)P2 in Panc1 cells in normal culture conditions (NC) and upon glutamine withdrawal (0 mM Gln) for 2 hours. The ratio of PI3K-C2γ-Lamp1-positive lysosomes was adjusted by the mean number of Lamp1-positive spots in every experimental condition (n=5).

(G) Pull-down of endogenous active Arf1 in WT/KO KPC cell lines upon glutamine withdrawal for 2 hours. Representative western blot images of active Arf1 pull-down assay probed with indicated antibodies (PD: pull down, TL: total lysate, n=5).

(H-I) Pull-down of endogenous active Arf1 in tumors taken from mice injected with WT/KO Panc1 (H) or KPC (I) cells. Representative western blot images of active Arf1 pull-down assay probed with indicated antibodies (PD: pull down, TL: total lysate, n=3).

Data are shown as mean ± SEM, by Student t test.

Figure S6.

PI3K-C2γ-derived PtdIns(3,4)P2 recruits Asap1 that inhibits Arf1 activity

(A) Quantification of Asap1 localization on Lamp1-positive lysosomes in WT/KO Panc1 cells. Results are shown as mean ± SEM (n = 10, *p < 0.05 by Student t test).

(B) Pull-down of WT and mutant Asap1 using PtdIns(3,4)P2-coated beads in Panc1 cells expressing mcherry, mcherry-Asap1 WT or mcherry-Asap1 R345L upon glutamine withdrawal for 2 hours. Representative western blot images of Asap1 pull-down assay probed with indicated antibodies (PD: pull down, TL: total lysate, n=5).

(C) Pull-down of WT and mutant Asap1 using PtdIns(4,5)P2-coated beads in Panc1 cells expressing mcherry, mcherry-Asap1 WT or mcherry-Asap1 R345L upon glutamine withdrawal for 2 hours. Representative western blot images of Asap1 pull-down assay probed with indicated antibodies (PD: pull down, TL: total lysate, n=5).

(D) Pull-down of endogenous active Arf1 in WT or Asap1 KO Panc1 cells expressing mcherry, mcherry-Asap1 WT or mcherry-Asap1 R345L upon glutamine withdrawal for 2 hours. Representative western blot images of active Arf1 pull-down assay and whole cell lysate probed with indicated antibodies (PD: pull down, TL: total lysate, n=5).

Figure S7.

PI3K-C2γ loss induces metabolic rewiring toward the anabolic use of glutamine

(A) KPC WT and KO cells were subjected to Seahorse XFe96 Mito Stress Test analysis and Oxygen Consumption Rate (OCR) was measured in real time in normal culture conditions or upon 1 hour of glutamine withdrawal (0 mM Gln 1 hr). Data are normalized on protein levels. Oligomycin is an adenosine triphosphate ATP synthase inhibitor (oligo), FCCP is the proton uncoupler carbonilcyanide p-triflouromethoxyphenylhydrazone, rotenone (Rot) is the respiratory complex I inhibitor, antimycin A (AntA) is with the respiratory complex III inhibitor (n=3).

(B-D) KPC WT/KO cells were subjected to Seahorse XFe96 Mito Stress Test analysis in normal culture conditions (2 mM Gln) or upon 1 hour of glutamine withdrawal (0 mM Gln 1 hr). Basal (B), maximal (C) and spare (D) OCR were measured and normalized on protein levels. Results are shown as mean ± SEM (n=3).

(E) Quantification of glucose consumption in normal culture conditions of KPC WT/KO cells. Results are shown as mean ± SEM (n=5).

(F) Quantification of lactate production in normal culture conditions of KPC WT/KO cell lines. Results are shown as mean ± SEM (n=5).

(G-H) Cell viability assay on KPC (G) and Panc1 (H) WT/KO cells at indicated glucose concentrations after 24hrs. Results are shown as mean ± SEM (n=5).

(I) Cell viability assay on KPC WT/KO cells at indicated glutamine concentrations after 24hrs. Results are shown as mean ± SEM (n=6).

(J) KPC WT/KO cell growth assay in normal culture condition (2 mM Gln) or upon glutamine depletion (0 mM Gln). Results are shown as mean ± SEM (#: KO 2 mM Gln vs KO 0 mM Gln; *: WT 0 mM Gln vs KO 0 mM Gln; n=6).

(K) Cell viability assay on KPC WT/KO cells in normal culture condition (2 mM Gln) or upon glutamine withdrawal (0 mM Gln) for 12 hrs and stimulated with BSA alone (BSA) or BSA-palmitate (BSA-Palm) for 24 hrs (n=6).

Data are shown as mean ± SEM, ANOVA followed by Bonferroni's post hoc test (B-D, G-K) or Student t test (E,F).

Figure S8.

PI3K-C2γ loss sensitizes to glutaminase inhibitors

(A) Cell viability assay on WT/KO Panc1 cells after 72 hrs treatment with BPTES at indicated concentrations (n=6).

(B) Cell viability assay on WT/KO KPC cells after 72 hrs treatment with BPTES at indicated concentrations (n=6).

(C) Cell viability assay on WT/KO KPC cells after 72 hrs treatment with CB-839 at indicated concentrations (n=6).

(D) Cell viability assay on WT/KO Panc1 cells after 48 hrs of treatment with CB 839, Everolimus or combination of the two drugs at indicated concentrations (n=6).

(E) Quantification of Caspase 3/7 activity in WT/KO Panc1 cells in normal culture condition (2 mM Gln) or upon glutamine withdrawal (0 mM Gln) and CB-839 or BPTES treatment for 24 hours (n=5).

(F-G) Western blot analysis of mTORC1 and Akt activation in WT/KO KPC (F) and Panc1 (G) cells upon Everolimus (EVR) or CB 839 treatment for 24 hours. Representative images of whole cell lysate probed with the indicated antibodies.

(H) Western blot analysis of phosphorylation status of AMPK in WT/KO Panc1 cells in normal culture condition (2 mM Gln, NT) or upon glutamine withdrawal (0 mM Gln) and CB-839 or BPTES treatment for 24 hours. Representative images of whole cell lysate probed with the indicated antibodies (top) and quantification of the pAMPK/AMPK ratio (bottom, n=5).

(I) Cell viability assay on WT/KO Panc1 cells after 48 hrs treatment with 1 μM Everolimus (EVR) in presence of 2 mM or 0.1 mM Glutamine (Gln, n=6).

Data are shown as mean ± SEM, ANOVA followed by Bonferroni's post hoc test.

Figure S9.

Glutaminase inhibitors reduce tumor growth in PI3K-C2γ-deficient xenograft models

(A) IHC assessment of the level of PCNA and pS6 in tumors taken from mice injected with WT/KO KPC cells treated with vehicle (NT), BPTES, Everolimus (EVR) or combination of the two drugs (COMBO) for 2.5 weeks.

(B) Coronal T_{2w} Magnetic Resonance images (B_0=7.1 T) of WT/KO KPC mice before the treatment or treated with vehicle (NT), BPTES, Everolimus (EVR) or combination of the two drugs (EVR) for 2.5 weeks. Light blu arrows indicate pancreatic tumor. Light blu arrow heads indicate tumor abdominal spread. Smallmlight blue small arrows indicate fuzzy edges.

(C) Kaplan-Meier curve for survival of KO KPC mice treated with either vehicle (NT) or combination (COMBO) of BPTES and Everolimus (n = 5 mice, p = 0.01 by Logrank test for trend).

(D) IHC assessment of the level of PCNA and pS6 in endogenous tumors taken from WT/KO KPC mice treated with vehicle (NT), BPTES, Everolimus (EVR) or combination of the two drugs (COMBO) for 2.5 weeks.

Figure S10

Graphical abstract

Schematic representation of the proposed working model and drug treatments.

Supplemental Figures

Figure S1

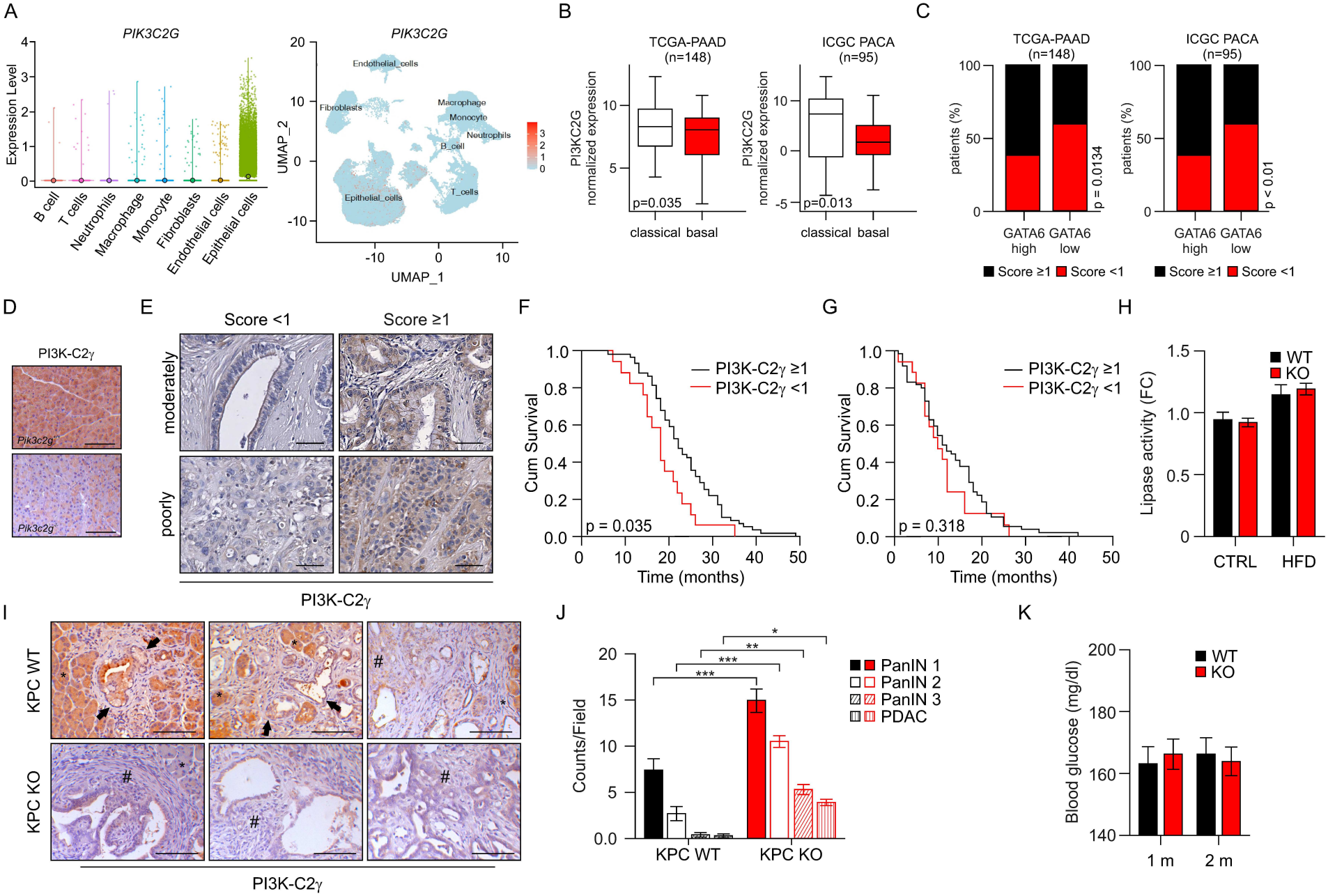
A
PIK3C2G
Expression Level
B cell
T cells
Neutrophils
Macrophage
Monocyte
Fibroblasts
Endothelial cells
Epithelial cells
UMAP_1
UMAP_2
B
TCGA-PAAD (n=148)
ICGC PACA (n=95)
PI3KC2G normalized expression
p=0.035
p=0.013
classical basal
C
patients (%)
p = 0.0134
p < 0.01
GATA6 high
GATA6 low
Score ≥1
Score <1
D
PI3K-C2γ
Pik3c2g-/-
Pik3c2g
E
Score <1
Score ≥1
moderately
poorly
PI3K-C2γ
F
Cum Survival
PI3K-C2γ ≥1
PI3K-C2γ <1
p = 0.035
Time (months)
G
p = 0.318
H
Lipase activity (FC)
WT
KO
CTRL
HFD
I
KPC WT
KPC KO
PI3K-C2γ
J
Counts/Field
PanIN 1
PanIN 2
PanIN 3
PDAC
KPC WT
KPC KO
K
Blood glucose (mg/dl)
1 m
2 m

Figure S2

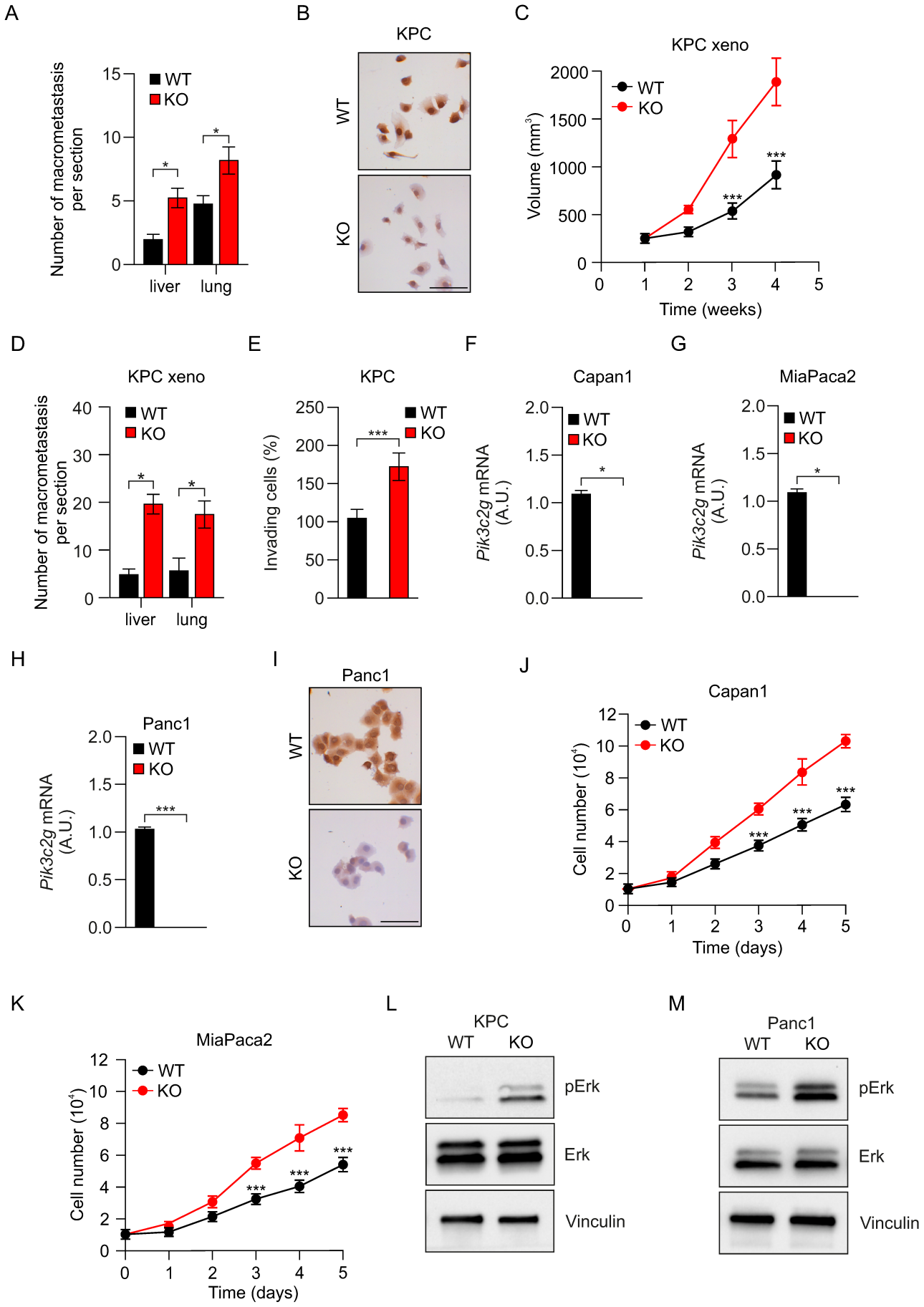
A
Number of macrometastasis per section
WT
KO
liver
lung
B
KPC
WT
KO
C
KPC xeno
Volume (mm3)
Time (weeks)
D
KPC xeno
Number of macrometastasis per section
E
KPC
Invading cells (%)
F
Capan1
Pik3c2g mRNA (A.U.)
G
MiaPaca2
H
Panc1
I
Panc1
J
Capan1
Cell number (10^4)
Time (days)
K
MiaPaca2
L
KPC
pErk
Erk
Vinculin
M
Panc1

Figure S3

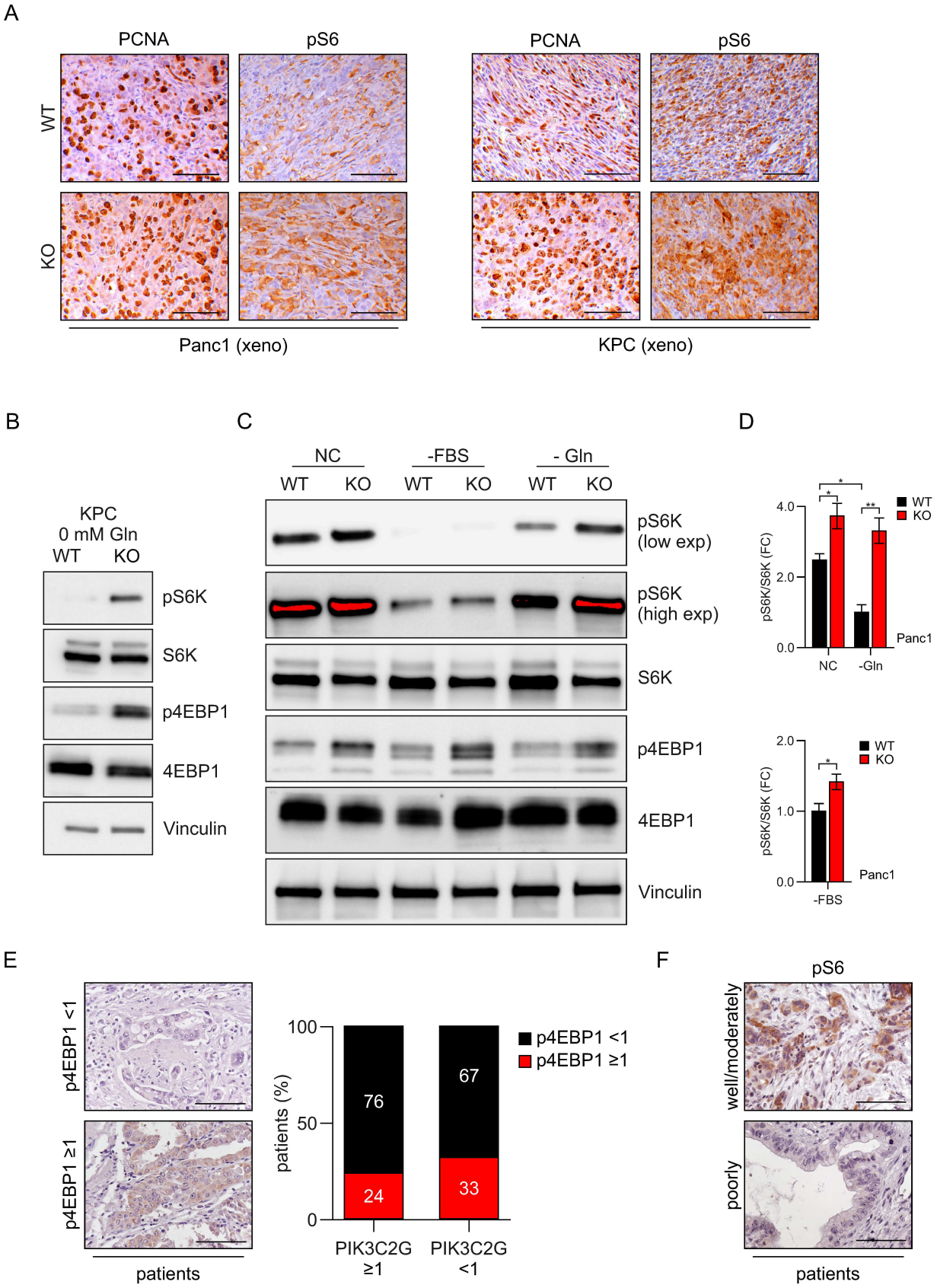
A
PCNA
pS6
PCNA
pS6
WT
KO
Panc1 (xeno)
KPC (xeno)
B
KPC
0 mM Gln
WT KO
pS6K
S6K
p4EBP1
4EBP1
Vinculin
C
NC
-FBS
- Gln
WT KO WT KO WT KO
pS6K (low exp)
pS6K (high exp)
S6K
p4EBP1
4EBP1
Vinculin
D
pS6K/S6K (FC)
WT
KO
Panc1
NC
-Gln
-FBS
E
p4EBP1 <1
p4EBP1 ≥1
patients
patients (%)
76
24
67
33
PIK3C2G ≥1
PIK3C2G <1
F
pS6
well/moderately
poorly
patients

Figure S4

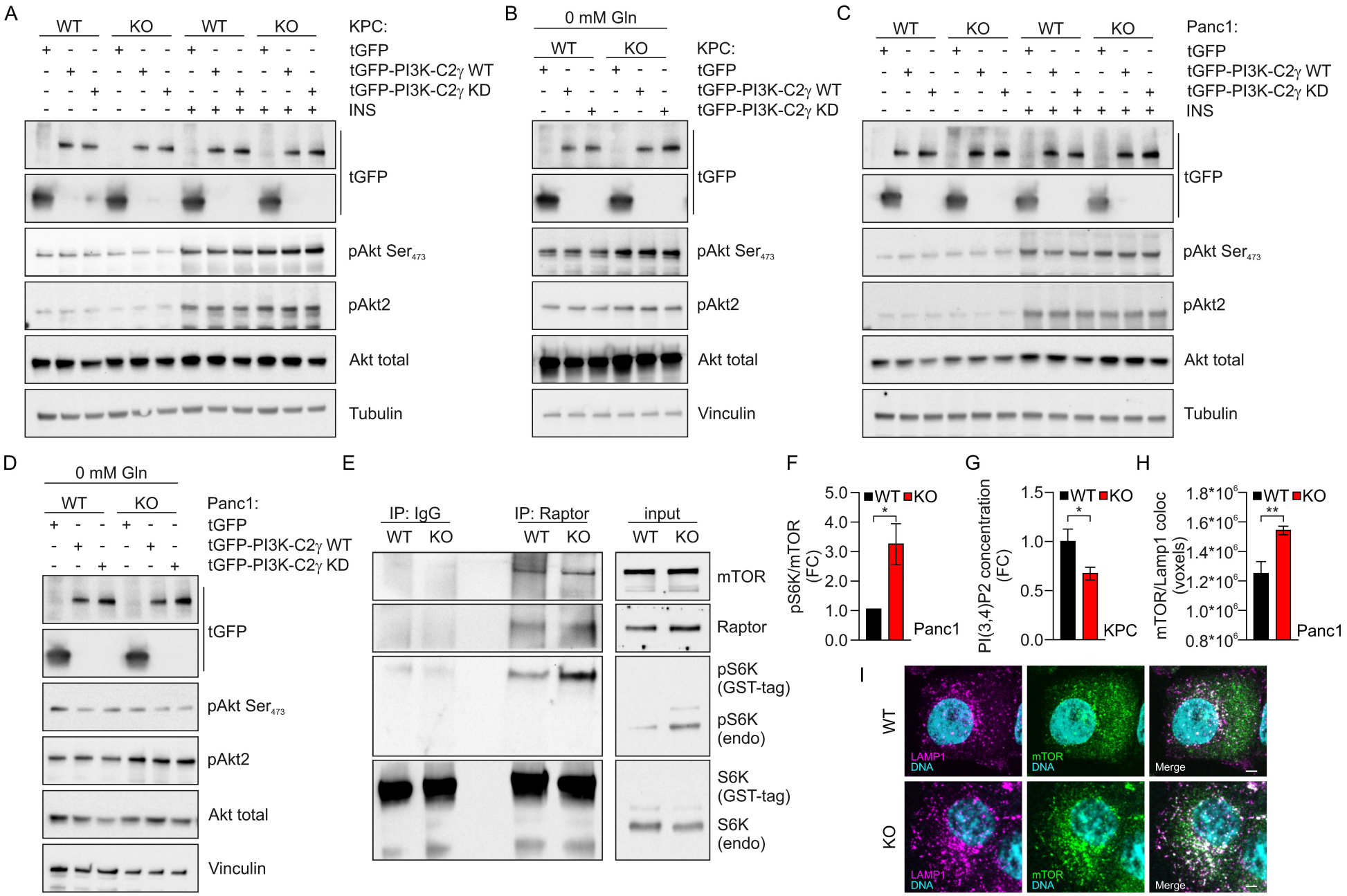
A
WT KO WT KO
KPC:
tGFP
tGFP-PI3K-C2γ WT
tGFP-PI3K-C2γ KD
INS
tGFP
pAkt Ser473
pAkt2
Akt total
Tubulin
B
0 mM Gln
WT KO
KPC:
tGFP
tGFP-PI3K-C2γ WT
tGFP-PI3K-C2γ KD
tGFP
pAkt Ser473
pAkt2
Akt total
Vinculin
C
WT KO WT KO
Panc1:
tGFP
tGFP-PI3K-C2γ WT
tGFP-PI3K-C2γ KD
INS
tGFP
pAkt Ser473
pAkt2
Akt total
Tubulin
D
0 mM Gln
WT KO
Panc1:
tGFP
tGFP-PI3K-C2γ WT
tGFP-PI3K-C2γ KD
tGFP
pAkt Ser473
pAkt2
Akt total
Vinculin
E
IP: IgG
IP: Raptor
input
WT KO WT KO WT KO
mTOR
Raptor
pS6K (GST-tag)
pS6K (endo)
S6K (GST-tag)
S6K (endo)
F
pS6K/mTOR (FC)
WT KO
Panc1
G
PI(3,4)P2 concentration (FC)
WT KO
KPC
H
mTOR/Lamp1 coloc (voxels)
WT KO
Panc1
I
WT
KO
LAMP1 DNA
mTOR DNA
Merge

Figure S5

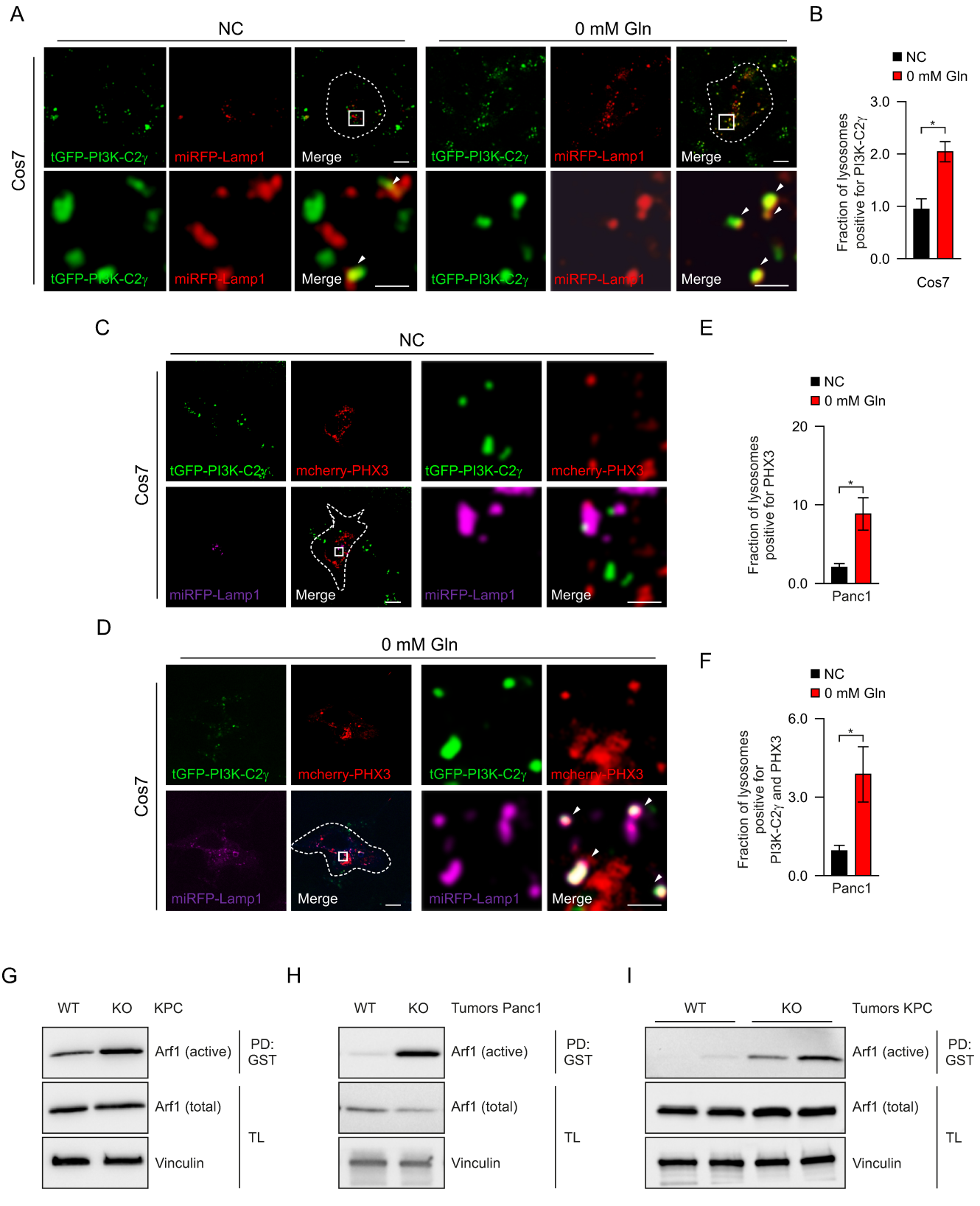
A
NC
0 mM Gln
Cos7
tGFP-PI3K-C2γ
miRFP-Lamp1
Merge
B
NC
0 mM Gln
Fraction of lysosomes positive for PI3K-C2γ
3.0
2.0
1.0
0.0
*
Cos7
C
NC
Cos7
tGFP-PI3K-C2γ
mcherry-PHX3
miRFP-Lamp1
Merge
D
0 mM Gln
E
NC
0 mM Gln
Fraction of lysosomes positive for PHX3
20
10
0.0
*
Panc1
F
NC
0 mM Gln
Fraction of lysosomes positive for PI3K-C2γ and PHX3
6.0
3.0
0.0
*
Panc1
G
WT
KO
KPC
Arf1 (active)
Arf1 (total)
Vinculin
PD: GST
TL
H
WT
KO
Tumors Panc1
I
WT
KO
Tumors KPC

Figure S6

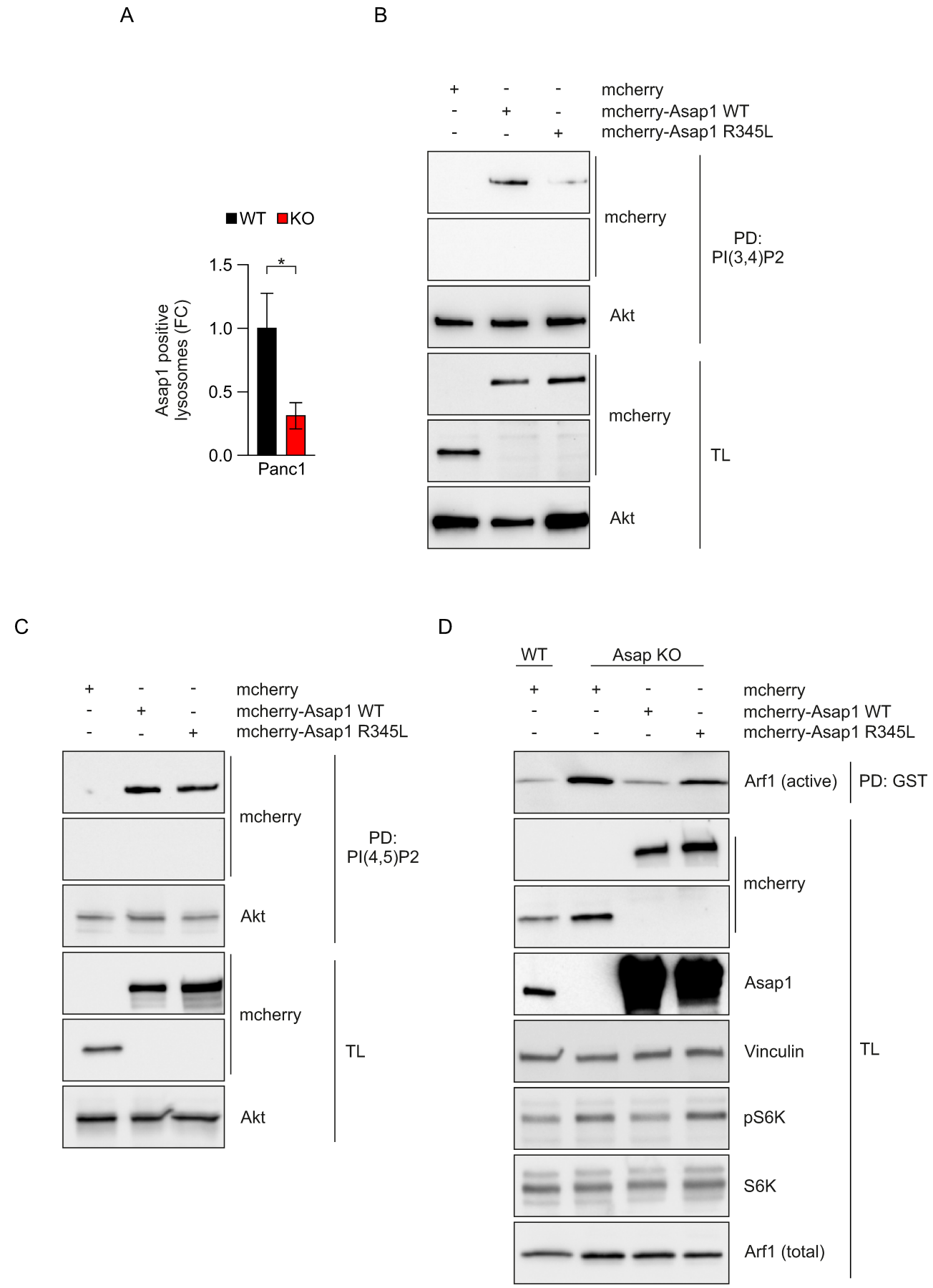
A
B
WT
KO
Asap1 positive lysosomes (FC)
1.5
1.0
0.5
0.0
*
Panc1
+ - - mcherry
- + - mcherry-Asap1 WT
- - + mcherry-Asap1 R345L
mcherry
Akt
PD: PI(3,4)P2
mcherry
Akt
TL
C
D
+ - - mcherry
- + - mcherry-Asap1 WT
- - + mcherry-Asap1 R345L
mcherry
Akt
PD: PI(4,5)P2
mcherry
Akt
TL
WT
Asap KO
+ + - - mcherry
- - + - mcherry-Asap1 WT
- - - + mcherry-Asap1 R345L
Arf1 (active)
PD: GST
mcherry
Asap1
Vinculin
pS6K
S6K
Arf1 (total)
TL

Figure S7

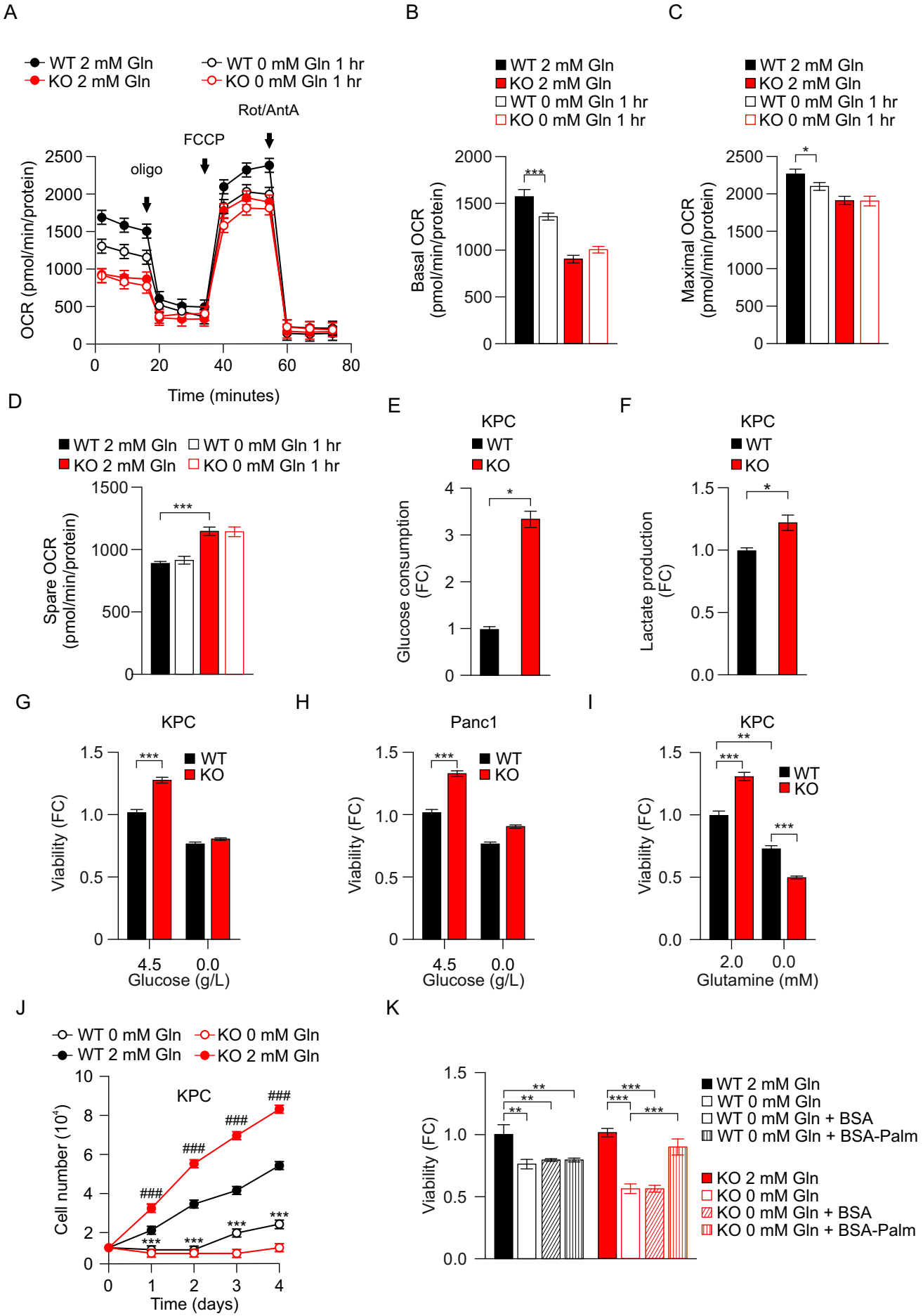
A
WT 2 mM Gln
KO 2 mM Gln
WT 0 mM Gln 1 hr
KO 0 mM Gln 1 hr
Rot/AntA
FCCP
oligo
OCR (pmol/min/protein)
Time (minutes)
B
Basal OCR (pmol/min/protein)
C
Maximal OCR (pmol/min/protein)
D
Spare OCR (pmol/min/protein)
E
KPC
Glucose consumption (FC)
F
Lactate production (FC)
G
KPC
Viability (FC)
Glucose (g/L)
H
Panc1
I
KPC
Glutamine (mM)
J
Cell number (10^4)
Time (days)
K
Viability (FC)
WT 2 mM Gln
WT 0 mM Gln
WT 0 mM Gln + BSA
WT 0 mM Gln + BSA-Palm
KO 2 mM Gln
KO 0 mM Gln
KO 0 mM Gln + BSA
KO 0 mM Gln + BSA-Palm

Figure S8

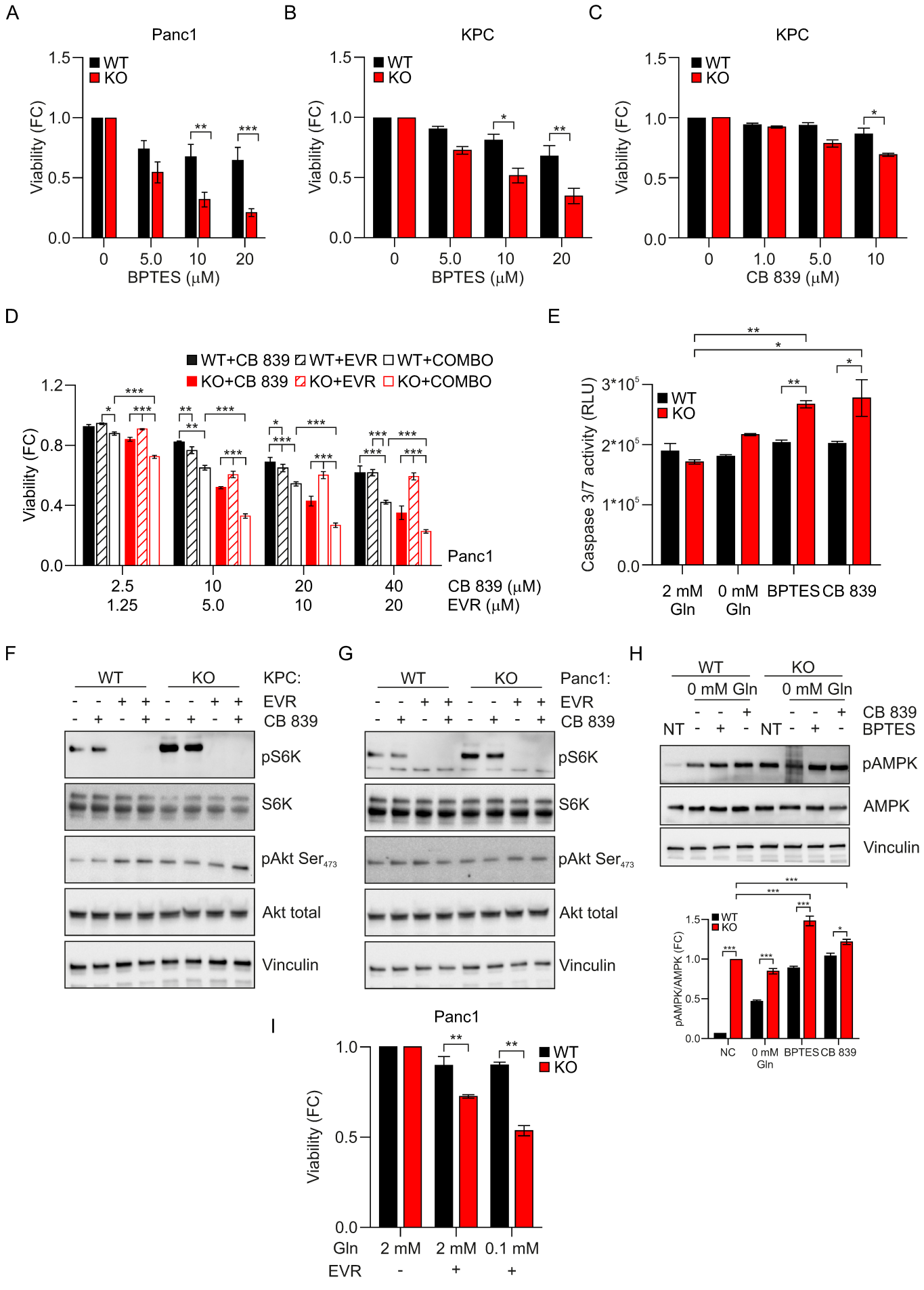
A
Panc1
WT
KO
Viability (FC)
BPTES (μM)
B
KPC
C
KPC
CB 839 (μM)
D
WT+CB 839 WT+EVR WT+COMBO
KO+CB 839 KO+EVR KO+COMBO
Panc1
CB 839 (μM)
EVR (μM)
E
Caspase 3/7 activity (RLU)
2 mM Gln
0 mM Gln
BPTES
CB 839
F
KPC:
EVR
CB 839
pS6K
S6K
pAkt Ser473
Akt total
Vinculin
G
Panc1:
H
0 mM Gln
NT
pAMPK
AMPK
Vinculin
pAMPK/AMPK (FC)
NC
I
Panc1
Gln
2 mM
0.1 mM

Figure S9

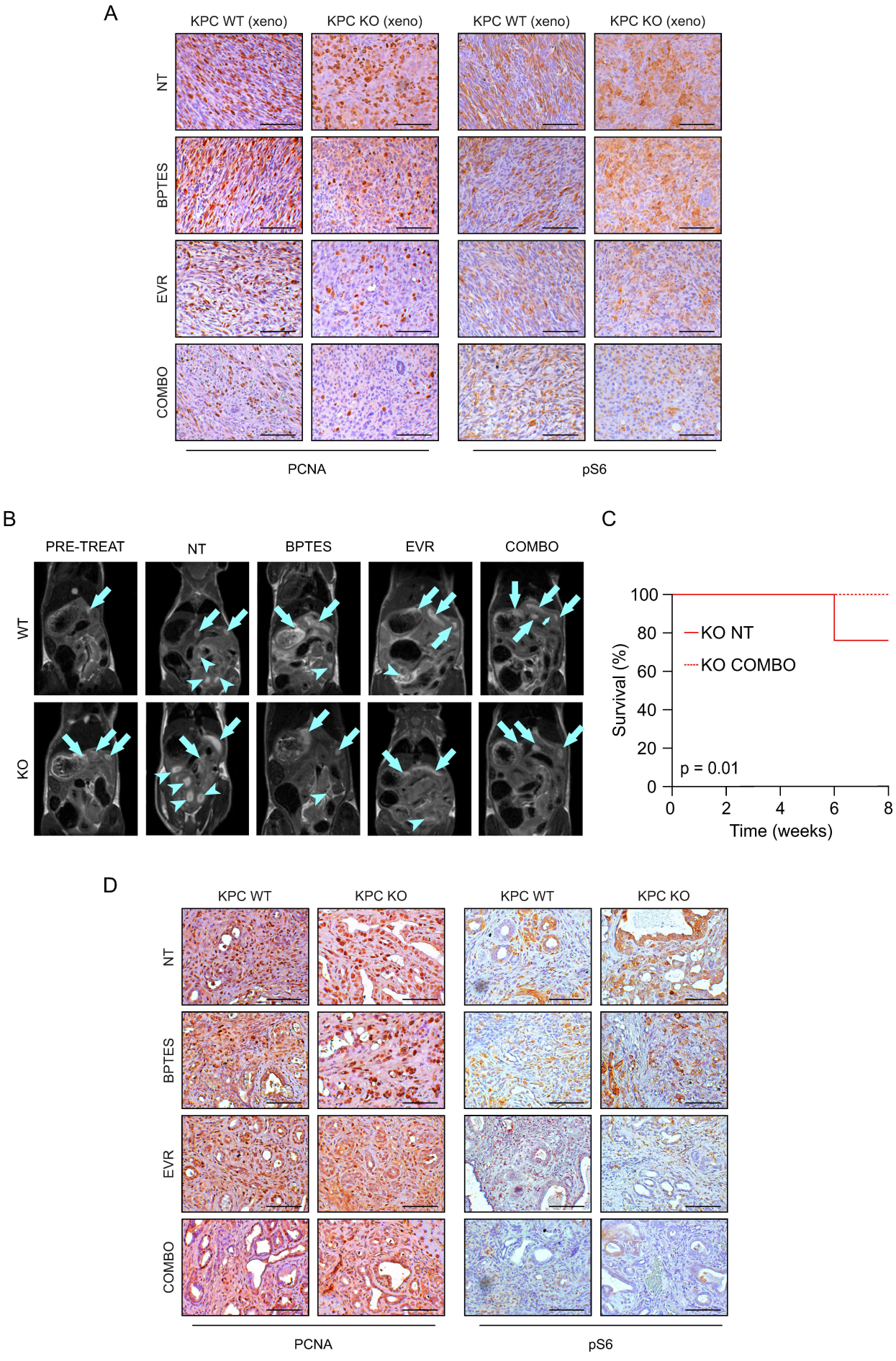
A
KPC WT (xeno)
KPC KO (xeno)
KPC WT (xeno)
KPC KO (xeno)
NT
BPTES
EVR
COMBO
PCNA
pS6
B
PRE-TREAT
NT
BPTES
EVR
COMBO
WT
KO
C
Survival (%)
100
80
60
40
20
0
KO NT
KO COMBO
p = 0.01
0
2
4
6
8
Time (weeks)
D
KPC WT
KPC KO
KPC WT
KPC KO
NT
BPTES
EVR
COMBO
PCNA
pS6

Figure S10

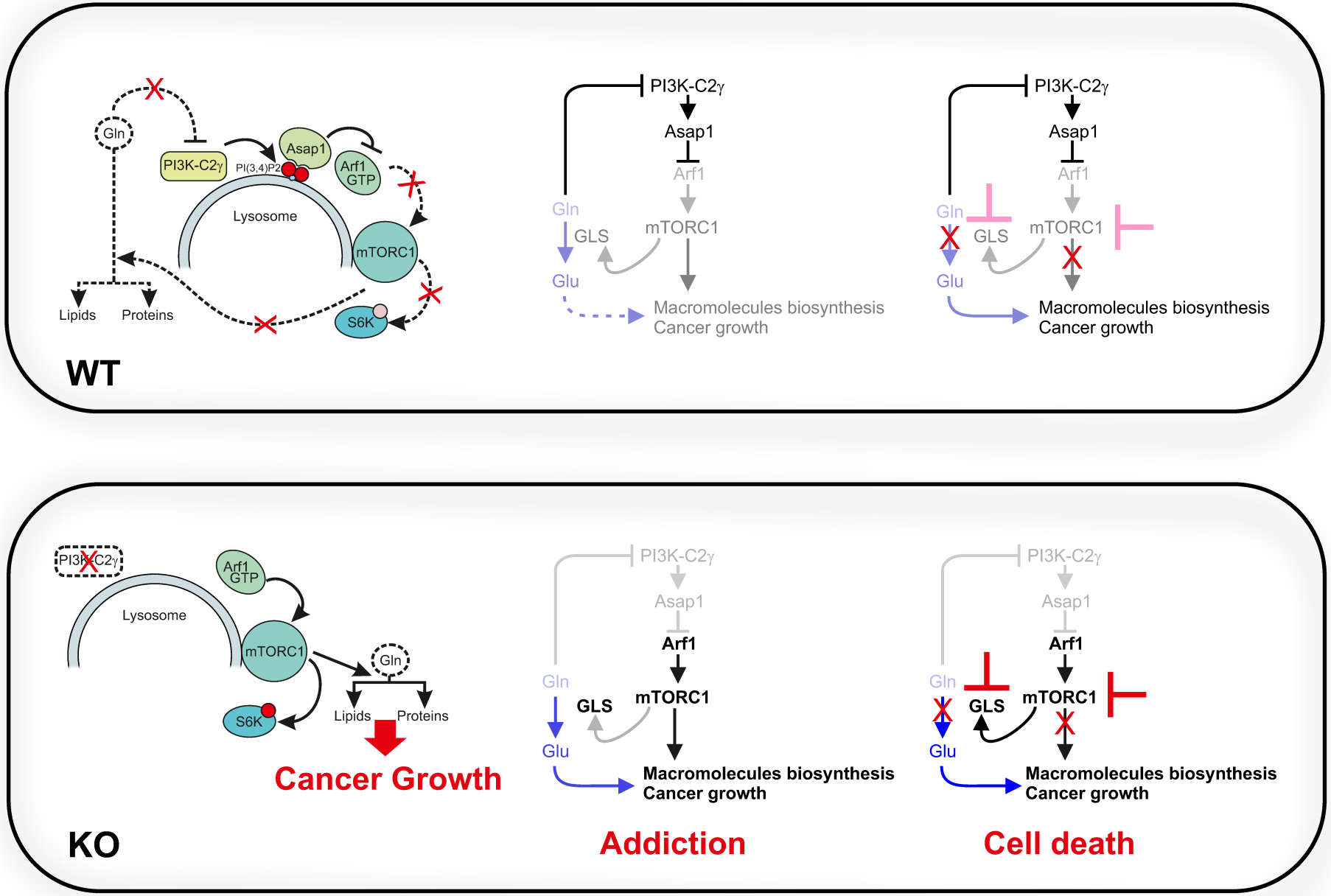
Gln
PI3K-C2γ
PI(3,4)P2
Asap1
Arf1 GTP
Lysosome
mTORC1
Lipids
Proteins
S6K
WT
PI3K-C2γ
Asap1
Arf1
Gln
GLS
mTORC1
Glu
Macromolecules biosynthesis
Cancer growth
PI3K-C2γ
Asap1
Arf1
Gln
GLS
mTORC1
Glu
Macromolecules biosynthesis
Cancer growth
PI3K-C2γ
Arf1 GTP
Lysosome
mTORC1
Gln
S6K
Lipids
Proteins
Cancer Growth
KO
PI3K-C2γ
Asap1
Arf1
Gln
GLS
mTORC1
Glu
Macromolecules biosynthesis
Cancer growth
Addiction
PI3K-C2γ
Asap1
Arf1
Gln
GLS
mTORC1
Glu
Macromolecules biosynthesis
Cancer growth
Cell death

Supplemental Material and methods

Gene expression analysis

For the integration of scRNA-seq datasets from PDAC tissues, we used the Harmony algorithm [1] via the R package *harmony* in order to account for the technical differences of the four datasets. The datasets (Peng et al. (primary PDAC=24, ncells=41964) [2], Lin et al. (primary PDAC=10, ncells=7752)[3], Chan-Seng-Yue et al. (primary PDAC=13, ncells=33970)[4] and Steele et al. (primary PDAC=16, ncells=42844)[5])) were first preprocessed individually using Seurat [6] for quality control and filtering (percent_mt_max=20, nFeature_min=500, nCount_min=500, nCount_max=50000) and then integrated using *harmony* function with default parameters and grouping by dataset variable. Cells were annotated with singleR package using the preloaded dataset HPCA from the celldex package [7] to stratify gene expression by cell population.

Histopathological analysis

For histological analysis, pancreata and tumors were fixed overnight in 4% paraformaldehyde (PFA), embedded in paraffin and cut into 3 μm thick sections. Sections were stained with hematoxylin and eosin (HE) following standard protocols and with specific antibodies: phospho-S6 Ser235/236 (#4858, Cell Signaling), PCNA 6D645 (sc-71858) and phospho-4E-BP1 Thr37/46 (#2855, Cell Signaling). Slides were dehydrated and mounted with moviol. Randomly selected areas were investigated under the light microscope (Olympus BH2), micro-photographed through digital imaging system then analyzed with ImageJ software. Two pathologists double-checked all the histological sections analyzed to exclude sarcomatoid pancreatic cancers that can be occasionally found in this model. Briefly, PanIN is a lesion that arises in native pancreatic ducts measuring <1 mm and not on a background of acinar-ductal metaplasia. PanIN lesions are graded as PanIN-1, 2 or 3 according to the cytological and architectural characteristics as described previously [8]. Quantitation of PanIN number was done on 5 20X fields of view from at least 4 mice.

Human pancreatic samples

PI3K-C2γ protein expression was evaluated in three independent cohorts of pancreatic ductal adenocarcinoma tumor samples. The first cohort (cohort #1) is composed by 73 pancreatic ductal adenocarcinoma tumor samples arranged in 4 TMA (Tissue MicroArray, Ethics approval number 1885 from the Integrated University Hospital Trust (AOUI) Ethics Committee (*Comitato Etico Azienda Ospedaliera Universitaria Integrata*) approved in their meeting of 17 November 2010 and documented by the ethics committee 52070/CE on 22 November 2010 and formalized by the Health Director of the AOUI on the order of the General Manager with protocol 52438 on 23 November 2010). The second cohort (cohort #2) consists of 76 pancreatic ductal adenocarcinoma tumor samples arranged in 3 TMA. The study protocol was approved by the local Ethics Committee at University Hospital of Pisa, Italy (Comitato di Bioetica, Azienda Ospedaliero-Universitaria Pisana, protocol number: 3909, July 3rd, 2013).

Four 1 mm tissue cores per case were included. Additional normal pancreatic parenchyma cores were used as controls and were integrated in the TMAs. Briefly, 4 μm FFPE sections were subjected to antigen retrieval in 10 mM citrate buffer (pH 6.0) for 5 min in pressure cooker at low pressure (106-110°C). Sections were than incubated overnight at 4°C with primary antibodies anti-PIK3C2G (1:300, ThermoFisher, Rockford, PA5-15239). Primary antibody was detected by incubation with HRP-labeled secondary antibody (Vector Laboratories, MP-7401) following by detection with 3,3' diaminobenzidine (Vector Laboratories, SK-4105). All slides were counterstained with Harris hematoxylin and then were scanned at 20x magnification and digitalized using the Aperio Scan-Scope XT Slide Scanner (Aperio Technologies). The immunolabeled slides were reviewed and scored blinded to any histopathological or clinical variables. The intensity of cytoplasmatic staining was scored in a three-tiered manner (scale:0=negative, 1+=weak staining, 2+=strong staining).

PI3K-C2γ protein expression was also evaluated in a third cohort (cohort #3) of 45 formalin-fixed and paraffin-embedded tissues of pancreatic ductal adenocarcinomas arranged in single TMA. The requirement for informed consent was waived because of the anonymous nature of the data and the descriptive nature of the immunohistochemical study. Briefly, 5 μm sections were stained with a rabbit polyclonal antibody raised against

93-123 amino acids from the N-terminal region of the human PI3K-C2γ protein (1:150; overnight incubation; cat. number PA5-15239; ThermoFisher, Rockford, IL). Antigen retrieval was performed by microwave treatment at 750 W (10 min) in 10 mM sodium citrate buffer (pH 6.0). The anti-rabbit EnVision kit (Agilent, Santa Clara, CA) was used for signal amplification. In control sections, the specific primary antibodies were replaced with isotype-matched immunoglobulins. The immunolabeled slides were reviewed and scored to any histopathological variables. Staining was evaluated by a molecular pathologist, assessing the amount of tumor and tissue loss, background, and overall interpretability. The intensity of cytoplasmatic staining was scored in a three-tiered manner (scale:0=negative, 1+=weak staining, 2+=strong staining). We attributed one, two, or three additional points if the percentage of positive cells was less than 25%, 25% to 50%, or greater than 50%, respectively. Neoplastic cells were always uniformly stained and positivity assessment was made by counting all the tumor cells present in three tumor cores.

Magnetic Resonance Imaging of mice

For the MRI experiments, mice were anesthetized *via* the intramuscular injection of tiletamine/zolazepam (Zoletil 100; Virbac, Milan, Italy) 20 mg/kg plus xylazine (Rompun; Bayer, Milan, Italy) 5 mg/kg using a 27-G syringe. MRI scans were acquired at 7.1 T on a Bruker Avance Neo 300 spectrometer equipped with the Micro 2.5 microimaging probe at room temperature. T_{2W} images were acquired using a standard RARE (Rapid Acquisition with Refocused Echoes) sequence with the following parameters (TR = 4000 ms, TE = 24 ms, RARE factor= 24, flip angle= 180°, number of averages= 6, FOV = 30 mm x 30 mm, slice thickness = 1 mm, matrix size 128 x 128).

Analysis of mice

Differences in survival were evaluated with Mantel-Cox log-rank test.

Serum biochemical analysis of *Pik3c2g*$^{+/+}$ and *Pik3c2g*$^{-/-}$ mice was performed using IDEXX Catalyst One instrument according to manufacturer instructions. For lipase levels, *Pik3c2g*$^{+/+}$ and *Pik3c2g*$^{-/-}$ mice were fed with Western/Fast Food diet (Envigo TD.120528) for 2 weeks and plasma lipase levels were measured with commercial kit (MAK046,

Sigma) according to manufacturer instructions. Blood glucose measurements of WT/KO KPC mice were performed as previously described in [9].

For orthotopic injections, WT/KO KPC cells (10^6 cells) were injected into 8 weeks old *Pik3c2g*$^{+/+}$ mice. About 2 weeks after inoculation, the tumors were measured twice a week using caliper and the volume was calculated according to the formula: $d*D^2/2$, where d stands for minor diameter and D for major diameter. All mice were culled at the end of treatment or when the tumor mass was >1500 mm^3. Tumor masses, lymph nodes, lungs and livers were collected for histological analysis.

For BPTES and/or Everolimus treatment, WT/KO KPC ($2*10^6$ cells/mice) and Panc1 ($4*10^6$ cells/mice) cells were injected subcutaneously in nu/nu CD1$^+$ mice. About 3 weeks after inoculation, the tumors were measured twice a week using caliper and the volume was calculated according to the formula: $d*D^2/2$, where d stands for minor diameter and D for major diameter. For treatment studies, mice with tumors in the 30–50 mm^3 size range or 5-6 weeks-old KPC mice were enrolled in a randomized fashion to either vehicle (PBS 10% DMSO) or BPTES (every 3 days, 12.5 mg/kg in PBS 10% DMSO) and/or Everolimus (daily, 1.5 mg/kg in PBS 5% Tween 20) for 2.5 weeks by intraperitoneal injection.

All experiments on mice have been performed in accordance with institutional and national guidelines and they conform to the relevant regulatory standards. The investigators were not blinded during experiments and outcome assessment.

Cell lines and primary cultures

Whole pancreas was collected from WT/KO KPC mice at late stage of tumor development. Tumors were finely chopped and then digested in DMEM medium (Gibco®), containing 1 mg/ml collagenase A (Roche Applied Science, Indianapolis, IN, USA). After 30 min at 37 °C, a mixture of epithelial-enriched fragments and non-epithelial single cells was obtained. The epithelial-enriched fraction, resulting from filtration through a 70 μm mesh (BD), was centrifuged at 1200 rpm for 5 min and plated on 10 cm dish. Cells were treated with 0.025% trypsin-EDTA (Gibco®) until fibroblasts elimination and cultured in DMEM High Glucose (Gibco®) 10% dialyzed Fetal Bovine Serum (dFBS, #26400-036, Invitrogen) supplemented with 2 mM glutamine (Invitrogen) and 5000 U/ml

Penicillin-Streptomycin (Gibco®). Three independent primary cell lines per genotype were used. Cells were detached using 0.1% trypsin-EDTA (Gibco®).

The human PC cell lines Capan1 (HBT-79), MiaPaca2 (CRL-1420), Panc1 (CRL-1469) and Cos7 (CRL-1651) cell lines were purchased from American Tissue Cell Culture (ATCC, Manassas, VA, USA) and maintained at 37 °C and in a 5% CO2 atmosphere in complete growing medium composed as follows: DMEM (Gibco®) High Glucose containing 2mM glutamine (Invitrogen), 5000 U/ml Penicillin-Streptomycin (Gibco®) and 10% heat-inactivated dialyzed fetal bovine serum (FBS) (dFBS, Invitrogen). Glucose free DMEM (containing 2 mM Gln) and glutamine-free DMEM were obtained from Invitrogen. A passage number of 20 was assumed for each cell line; after these 20 passages, a new culture was started with the stock constituted after the reception of the cells from ATCC. Human cell lines authentication was performed by BMR Genomics. All cell lines were routinely tested for Mycoplasma contamination using PCR.

Cell culture and growth

For growth assays via cell counts, KPC and Panc1 cells were plated into 96-well plates in quadruplicate at $5 * 10^3$ cells/well and counted with CellTiter-Fluor® Cell Viability Assay (Promega). Fluorescence was recorded at indicated time point.

For drug treatment, cells were seeded in quadruplicate at $5 * 10^3$ cells per 96-well plate; vehicle, Everolimus (11597, Cayman Chemical), CB-839 (22038, Cayman Chemical) or BPTES (S7753, Aurogene) were added the day after seeding in complete growing medium. Cells were counted at the indicated time point with CellTiter-Fluor® Cell Viability Assay (Promega). Cell survival was considered as the ratio of live cells after treatment compared with WT live cells treated with vehicle alone.

For glutamine deprivation, cells were seeded in complete growing medium. 16 hours after seeding, cells were washed twice with PBS and DMEM High Glucose, no glutamine containing 10% dFBS or DMEM High Glucose, no glutamine containing 10% dFBS supplemented with either 2 mM or 10 mM glutamine (Invitrogen) was added for 2 hours or otherwise indicated.

For metabolite treatment, 16 hours post seeding, complete growing medium was replaced with glutamine-free medium supplemented with 10% dFBS. After 16 hours of glutamine withdrawal, metabolites were added at the indicated concentrations. Dimethyl

α-KetoGlutarate, Dimethyl L-glutamate and BSA-conjugated palmitate were purchased from Sigma. After 24 hours, cells were counted with CellTiter-Fluor® Cell Viability Assay (Promega). Cell survival was considered as the ratio of live cells after treatment compared with WT live cells in normal growing conditions (2 mM glutamine).

Caspase activity was measured using Caspase-Glo 3/7 assay kit following the manufacturer's protocol (Promega).

Plasmids

All constructs were verified by restriction digest and automated DNA sequencing. KPC and Panc-1 cells were transfected using X-tremeGENE™ HP DNA Transfection Reagent (XTGHP-RO, Roche) and Cos7 cells with Lipofectamine® 2000 (Life Technologies) according to manufacturer's instructions.

The following plasmids were used: PIK3C2G-tGFP (OriGene Technologies, cat. n. RG217086), ASAP1-mCherry (Vector Builder, NM_001362924.1), pLAMP1-miRFP703 (a gift from Vladislav Verkhusha, Addgene plasmid #79998; http://n2t.net/addgene:79998; RRID:Addgene_79998), NES-EGFP-cPHx3 and NES-mCherry-cPHx3 (a kind gift of prof. Gerry Hammond, University of Pittsburgh).

PIK3C2G Kinase Dead (D1051A) [10, 11] mutant was generated by site directed mutagenesis (Quikchange Lightning kit, Agilent) using the following pair of primers: CGGGCCACATGTTTCATATTGCCTTTGGAAAATTC and GAATTTTCCAAAGGCAATATGAAACATGTGGCCCG and was verified by sequencing.

ASAP1 R345L mutant [12, 13] was generated by site directed mutagenesis (Quikchange Lightning kit, Agilent) using the following pair of primers: ATCCGGAAAGTATGGCAGAGGCTAAAGTGTTCAGTCAAGAATGGG and CCCATTCTTGACTGAACACTTTAGCCTCTGCCATACTTTCCGGAT and was verified by sequencing.

CRISPR/Cas9

For CRISPR/Cas9 mediated gene editing, target sequences were designed via a gRNA design tool (Feng Lab CRISPR Design Web Tool at http://crispr.mit.edu). Each sequence was cloned into the PX459-SpCas9 plasmid to express the Cas9 and single guide RNAs (sgRNAs). The following primers were used: for *PIK3C2G*

AAACTCAATTTCACTCTCGTAGTGC and CACCGCACTACGAGAGTGAAATTGA, for *Asap1*: CACCGCAGGAACACCGTCACGCTGC and AAACGCAGCGTGACGGTGTTCCTGC.

Plasmid was transfected in Capan1, MiaPaca2 and Panc1 cells and single cell dilution was performed in order to select 3 clones per condition.

PtdIns(3,4)P2 ELISA assay

WT/KO KPC and Panc1 were plated in a 15 cm dish in complete growing media, otherwise indicated. Acidic lipids extraction and quantification of PI(3,4)P2 were performed using ELISA kits (K-3800, Echelon Biosciences), according to manufacturer instructions.

Live cell imaging

5 * 10^4 Cos7 or 7 * 10^4 Panc1 cells were plated in 8 well μ-Slide and transfected with PIK3C2G-tGFP, NES-EGFP-cPHx3, NES-mCherry-cPHx3, pLAMP1-miRFP703, pARF1-CFP or mCherry-Asap1. 48 hours post-transfection, cells were washed twice and complete growing medium was replaced with glutamine-free medium supplemented with 10% dFBS alone or with 2 mM glutamine (Invitrogen), for 2 hours before image acquisition. Image acquisition was performed with Leica TCS SP8 confocal system (Leica Microsystems) equipped with a HCX PL APO 63×/1.4 NA oil-immersion objective. Images were acquired on the three coordinates of the space (XYZ planes) with a resolution of 0.09 μm x 0.09 μm x 0.6 μm and were processed and analysed with ImageJ software (Rasband, W.S., U.S. National Institutes of Health, Bethesda, MA). In particular, images were pre-processed with background subtraction and Gaussian blur and segmented using intensity thresholding; binary images were post-processed to improve spot detection, finally, colocalization is analysed with JACoP plugin [14] using an object based method (centres-particles coincidence).

Immunofluorescence

Immunofluorescence was performed as previously described [15]. The following primary antibodies were used: CD107a/LAMP1 (H4A3) (Mouse, 555798, BD Pharmingen) and mTOR (7C10) (Rabbit, #2983, Cell Signaling). Number of colocalized

voxels (mTOR green and Lamp1 Magenta) has been calculated by using ImarisColoc software.

Protein analysis

Cells were homogenized in lysis buffer (120 mM NaCl, 50 mM Tris-HCl pH=8, 1% Triton X-100) supplemented with 25x protease inhibitor cocktail (Roche), 50 mM sodium fluoride and 1 mM sodium orthovanadate. Lysates were cleared by centrifugation at 13,000 rpm for 10 min at 4°C. Protein concentration was determined by Bradford method and supernatants were analyzed for immunoblotting with the indicated antibodies. Membranes probed with the indicated antibodies were then incubated with HRP-conjugated secondary antibodies (anti-mouse used 1:10000, anti-rabbit 1:5000, Sigma or anti-rabbit light chain specific, 211-032-171, Jackson Lab) and developed with enhanced chemiluminescence (Clarity Western ECL Substrate, 1705060, Biorad).

The following primary antibodies were used: DDEF1/Asap1 (mouse, sc-374410; Santa Cruz), Arf1 (Rabbit, 16121, Thermo Scientific), Phospho-p70 S6 Kinase (Thr389) (Rabbit, #9234, Cell Signaling), p70 S6 Kinase (Rabbit, #9202, Cell Signaling), mTOR (7C10) (Rabbit, #2983, Cell Signaling), Raptor (24C12) (Rabbit, #2280S, Cell Signaling), anti-beta Tubulin (Rabbit, ab6046, Abcam), turboGFP (clone OTI2H8, Mouse, TA150041, OriGene), mCherry (Rabbit, #43590, Cell Signaling), Phospho-Akt (Ser473) (Rabbit, #9271, Cell Signaling), Phospho-Akt2 (Ser474) (D3H2) (Rabbit, #8599, Cell Signaling), Akt (pan) (40D4) (Mouse, #2920, Cell Signaling), pAMPKalpha T172 D4D6D (Rabbit, #50081, Cell Signaling), AMPK-alpha D5A2 (#5831, Cell Signaling) and Vinculin (Mouse, sc-25336), Phospho-4E-BP1 (Thr37/46) (236B4) (Rabbit, #2855, Cell Signaling), 4E-BP1 (53H11) (Rabbit, #9644, Cell Signaling), Phospho-p44/42 MAPK (Erk1/2) (Thr202/Tyr204) (20G11) (Rabbit, #4376, Cell Signaling), p44/42 MAPK (Erk1/2) (Rabbit, #9102, Cell Signaling).

mTORC1 kinase assay was performed as previously described [16]. Briefly, cells were homogenized in ice-cold lysis buffer (40 mM HEPES [pH 7.4], 2 mM EDTA, 0.3% CHAPS supplemented with 25x protease inhibitor cocktail (Roche), 50 mM sodium fluoride and 1 mM sodium. Lysates were cleared by centrifugation at 13,000 rpm for 10 min at 4°C. For immunoprecipitation, anti-Raptor antibody (Rabbit, #2280, Cell Signaling) or Rabbit IgG isotype control (#10500C, Invitrogen) was added to the lysates

and incubated with rotation for 2 hrs at 4°C. 10 μl of G Sepharose was added for an additional 30 min. Immunoprecipitates were washed five times with low salt wash buffer (40 mM HEPES [pH 7.4], 150 mM NaCl, 2 mM EDTA, 0.3% CHAPS). For kinases assay, immunoprecipitates were then washed twice in 25 mM HEPES (pH 7.4), 20 mM potassium chloride. Kinase assays were performed for 5 min at 30°C in a final volume of 15 μl consisting of mTORC1 kinase buffer (25 mM HEPES [pH 7.4], 50 mM KCl, 10 mM MgCl2, 250 μM ATP) and 100 ng GST tagged human P70S6K (SRP5055, Sigma) as substrate. Reactions were stopped by the addition of 20 μl of sample buffer, boiling for 10 min and analyzed by SDS-PAGE and immunoblotting.

Active Arf1 pull-down experiment was performed according to manufacturer instructions (16121, Thermo Scientific). Briefly, 16 hours post-seeding or 48 hours post transfection with PIK3C2G-tGFP WT or PIK3C2G-tGFP KD or tGFP alone, Panc1 cells were washed twice with PBS and media were replaced with complete growing media or glutamine deprived media for 2 hours, then cells were harvested and homogenized in lysis buffer supplemented with 25x protease inhibitor cocktail (Roche), 50 mM sodium fluoride and 1 mM sodium orthovanadate. 500 μg of lysates were incubated with 30 μl of Glutathione Agarose Resin and 30 μg of GST-GGA3-RBD Fusion Protein for 1 hour at 4 °C on a rotating rack. Samples were collected by centrifugation (3000 g for 1 min) and washed six-times with lysis buffer. Bound protein complexes were then eluted by adding 30 μl Laemli sample buffer.

PI(3,4)P2 (P-B034a, Echelon Biosciences) and PI(4,5)P2 (P-B045a, Echelon Biosciences) pull down experiments were performed according to manufacturer instruction. Briefly, 24 hours post transfection with Asap1-mCherry WT, Asap1-mCherry R345L or mCherry alone, complete growing medium was replaced with glutamine-free medium supplemented with 10% dFBS. After 2 hours of glutamine withdrawal, Panc1 cells were harvested and homogenized in lysis buffer (10 mM HEPES, pH 7.4, 150 mM NaCl, 0.25% Igepal) supplemented with 25x protease inhibitor cocktail (Roche), 50 mM sodium fluoride and 1 mM sodium orthovanadate. 2 mg of lysates were incubated with 30 μl of PI(3,4)P2 or PI(4,5)P2 beads for 3 hours at 4 °C on a rotating rack. Samples were collected by centrifugation (3000 g for 1 min) and washed six-times with lysis buffer. Bound protein complexes were then eluted by adding 30 μl Laemli sample buffer.

Metabolic assay

A total of 2 * 10^3 cells per well were seeded in 96-well plates, cells counted using Cell Titer Fluor, while the supernatants of cell culture medium were collected. The media were assayed for glucose and lactate levels by using Biosen C-Line analyzer according to the manufacturer's instruction. The glucose consumption and lactate production were normalized to cell number. The experiments were performed with three replicates and repeated for three times.

Seahorse XFe96 Metabolic Assay

1.5 - 2 * 10^4 KPC WT and KO cells were seeded per well in XFe96 cell culture plates (5-10 technical replicates) in the presence or absence of 2 mM glutamine and subjected to the Seahorse XF Cell Mito Stress Test. 24 hours post seeding, routine culture medium was replaced with XF base medium supplemented with 25 mM glucose and 1 mM sodium pyruvate ± 2 mM glutamine. Cells were incubated for 1 hour at 37°C in a non-CO_2 incubator to allow cells equilibrating with the XF base medium. Mito Stress Test analysis measures basal respiration, maximal respiration, and the cells ability to exploit the mitochondrial oxidative metabolism. The analysis was performed in real-time by recording the value of OCR (Oxygen Consumption Rate) and ECAR (Extracellular Acidification Rate) after serial injections of drugs that affect the electron transport chain: oligomycin (1 μM), FCCP (carbonyl cyanide-4 (trifluoromethoxy) phenylhydrazone) (1 μM) and a mix of Rotenone/Antimycin A (0.5 μM) as previously described in [17]. Basal respiration is calculated as last rate OCR measurement before oligomycin injection – non-mitochondrial oxygen consumption rate. Maximal respiration is calculated as the maximum rate OCR measurement after FCCP injection – non-mitochondrial oxygen consumption rate. The results were normalized on protein content.

Radioactive assays

1 * 10^5 KPC WT and KO cells were seeded in 6-well culture plates in their routine culture medium. To analyze the incorporation of uniformly (U) radiolabeled ^{14}C-glutamine into proteins and lipids, culture medium was supplemented with 0.05 μCi/mL ^{14}C-glutamine (Perkin Elmer) 24 hours prior to the experiment. For radioactive incorporation into proteins, cells were washed in ice cold PBS and resuspended in 20% trichloroacetic

acid, then moved in ice for 30 minutes and centrifuged at 10,000 rpm for 10 minutes at 4°C. Pellet was resuspended in dH_2O, transferred into a scintillation vial and counted on the scintillation counter. For radioactive incorporation into lipids, cells were washed three times in ice cold PBS, lysed with methanol, and resuspended first in 4 volumes of a CHCl3:MeOH (1:1) solution and then in an additional volume of dH_2O. Samples were centrifuged at 1,000 rpm for 5 minutes at room temperature and the lower phases were collected into a scintillation vial and counted on the scintillation counter as previously described in [18]. Protein quantification was used to normalize all the radioactive signals.

Statistical Analysis

Prism software (GraphPad) was used for statistical analysis. Significance was calculated with Student t test and one- or two-way analysis of variance tests (ANOVA) followed by Bonferroni's post hoc analysis, or Mantel Cox log-rank test where appropriate. Values are reported as the mean ± standard error of the mean (SEM). $p<0.05$ was considered statistically significant (∗), $p<0.01$ very significant (∗∗) and extremely significant $p<0.001$ (∗∗∗).

References

1 Korsunsky I, Millard N, Fan J, Slowikowski K, Zhang F, Wei K*, et al.* Fast, sensitive and accurate integration of single-cell data with Harmony. Nature methods 2019;**16**:1289-96.

[Peng dataset] 2 Peng J, Sun BF, Chen CY, Zhou JY, Chen YS, Chen H*, et al.* Single-cell RNA-seq highlights intra-tumoral heterogeneity and malignant progression in pancreatic ductal adenocarcinoma. Cell research 2019;**29**:725-38 https://doi.org/10.1038/s41422-019-0195-y.

[Lin dataset] 3 Lin W, Noel P, Borazanci EH, Lee J, Amini A, Han IW*, et al.* Single-cell transcriptome analysis of tumor and stromal compartments of pancreatic ductal adenocarcinoma primary tumors and metastatic lesions. Genome medicine 2020;**12**:80. https://doi.org/10.1186/s13073-020-00776-9

[Chan-Seng-Yue dataset] 4 Chan-Seng-Yue M, Kim JC, Wilson GW, Ng K, Figueroa EF, O'Kane GM*, et al.* Transcription phenotypes of pancreatic cancer are driven by genomic events during tumor evolution. Nature genetics 2020;**52**:231-40. https://doi.org/10.1038/s41588-019-0566-9

[Steele dataset] 5 Steele NG, Carpenter ES, Kemp SB, Sirihorachai V, The S, Delrosario L*, et al.* Multimodal Mapping of the Tumor and Peripheral Blood Immune Landscape in Human Pancreatic Cancer. Nature cancer 2020;**1**:1097-112. https://doi.org/10.1038/s43018-020-00121-4

[Stuart dataset] 6 Stuart T, Butler A, Hoffman P, Hafemeister C, Papalexi E, Mauck WM, 3rd*, et al.* Comprehensive Integration of Single-Cell Data. Cell 2019;**177**:1888-902 e21. https://doi.org/10.1016/j.cell.2019.05.031

[Aran dataset] 7 Aran D, Looney AP, Liu L, Wu E, Fong V, Hsu A*, et al.* Reference-based analysis of lung single-cell sequencing reveals a transitional profibrotic macrophage. Nature immunology 2019;**20**:163-72. https://doi.org/10.1038/s41590-018-0276-y

8 Hruban RH, Adsay NV, Albores-Saavedra J, Anver MR, Biankin AV, Boivin GP*, et al.* Pathology of genetically engineered mouse models of pancreatic exocrine cancer: consensus report and recommendations. Cancer research 2006;**66**:95-106.

9 Braccini L, Ciraolo E, Campa CC, Perino A, Longo DL, Tibolla G*, et al.* PI3K-C2gamma is a Rab5 effector selectively controlling endosomal Akt2 activation downstream of insulin signalling. Nature communications 2015;**6**:7400.

10 Alliouachene S, Bilanges B, Chicanne G, Anderson KE, Pearce W, Ali K*, et al.* Inactivation of the Class II PI3K-C2beta Potentiates Insulin Signaling and Sensitivity. Cell reports 2015;**13**:1881-94.

11 Valet C, Chicanne G, Severac C, Chaussade C, Whitehead MA, Cabou C*, et al.* Essential role of class II PI3K-C2alpha in platelet membrane morphology. Blood 2015;**126**:1128-37.

12 Kam JL, Miura K, Jackson TR, Gruschus J, Roller P, Stauffer S*, et al.* Phosphoinositide-dependent activation of the ADP-ribosylation factor GTPase-activating protein ASAP1. Evidence for the pleckstrin homology domain functioning as an allosteric site. The Journal of biological chemistry 2000;**275**:9653-63.

13 Wullschleger S, Wasserman DH, Gray A, Sakamoto K, Alessi DR. Role of TAPP1 and TAPP2 adaptor binding to PtdIns(3,4)P2 in regulating insulin sensitivity defined by knock-in analysis. Biochem J 2011;**434**:265-74.
14 Bolte S, Cordelieres FP. A guided tour into subcellular colocalization analysis in light microscopy. Journal of microscopy 2006;**224**:213-32.
15 Marat AL, Wallroth A, Lo WT, Muller R, Norata GD, Falasca M*, et al.* mTORC1 activity repression by late endosomal phosphatidylinositol 3,4-bisphosphate. Science 2017;**356**:968-72.
16 Sancak Y, Thoreen CC, Peterson TR, Lindquist RA, Kang SA, Spooner E*, et al.* PRAS40 is an insulin-regulated inhibitor of the mTORC1 protein kinase. Molecular cell 2007;**25**:903-15.
17 Lorito N, Bacci M, Smiriglia A, Mannelli M, Parri M, Comito G*, et al.* Glucose Metabolic Reprogramming of ER Breast Cancer in Acquired Resistance to the CDK4/6 Inhibitor Palbociclib(.). Cells 2020;**9**.
18 Bacci M, Lorito N, Ippolito L, Ramazzotti M, Luti S, Romagnoli S*, et al.* Reprogramming of Amino Acid Transporters to Support Aspartate and Glutamate Dependency Sustains Endocrine Resistance in Breast Cancer. Cell reports 2019;**28**:104-18 e8.